HHS Public Access

Author manuscript

Cell Rep. Author manuscript; available in PMC 2023 December 13.

Published in final edited form as:

Cell Rep. 2023 August 29; 42(8): 112846. doi:10.1016/j.celrep.2023.112846.

Phospholipids can regulate complex I assembly independent of their role in maintaining mitochondrial membrane integrity

Anjaneyulu Murari[1], **Shauna-Kay Rhooms**[1], **Divya Vimal**[1], **Kaniz Fatima Binte Hossain**[1], **Sanjay Saini**[1], **Maximino Villanueva**[1], **Michael Schlame**[2], **Edward Owusu-Ansah**[1,3,*]

[1]Department of Physiology and Cellular Biophysics, Columbia University Irving Medical Center, New York, NY 10032, USA

[2]Departments of Anesthesiology and Cell Biology, New York University Grossman School of Medicine, New York, NY 10016, USA

[3]Lead contact

SUMMARY

Several phospholipid (PL) molecules are intertwined with some mitochondrial complex I (CI) subunits in the membrane domain of CI, but their function is unclear. We report that when the *Drosophila melanogaster* ortholog of the intramitochondrial PL transporter, STARD7, is severely disrupted, assembly of the oxidative phosphorylation (OXPHOS) system is impaired, and the biogenesis of several CI subcomplexes is hampered. However, intriguingly, a restrained knockdown of STARD7 impairs the incorporation of NDUFS5 and NDUFA1 into the proximal part of the CI membrane domain without directly affecting the incorporation of subunits in the distal part of the membrane domain, OXPHOS complexes already assembled, or mitochondrial cristae integrity. Importantly, the restrained knockdown of STARD7 appears to induce a modest amount of cardiolipin remodeling, indicating that there could be some alteration in the composition of the mitochondrial phospholipidome. We conclude that PLs can regulate CI biogenesis independent of their role in maintaining mitochondrial membrane integrity.

Graphical Abstract

*Correspondence: eo2364@cumc.columbia.edu.

AUTHOR CONTRIBUTIONS

A.M., S.-K.R., D.V., K.F.B.H., S.S., M.V., and E.O.-A. performed all the experiments except the lipidomics experiment. M.S. performed the lipidomics experiments. A.M., S.-K.R., D.V., K.F.B.H., S.S., M.S., and E.O.-A. analyzed and discussed results. E.O.-A. conceived and managed the project. E.O.-A. wrote the manuscript and got feedback from the other authors.

SUPPLEMENTAL INFORMATION

Supplemental information can be found online at https://doi.org/10.1016/j.celrep.2023.112846.

DECLARATION OF INTERESTS

The authors declare no competing interests.

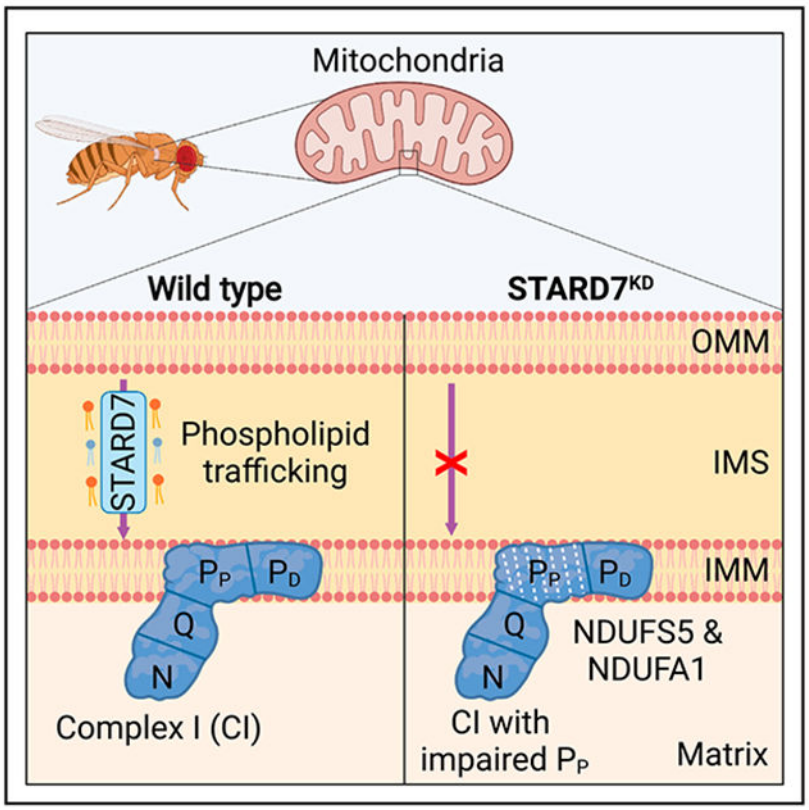

In brief

Murari et al. show that a restrained inactivation of the phospholipid transporter, STARD7, in fruit fly (*Drosophila melanogaster*) flight muscles can impair specific steps in the biogenesis of complex I without altering mitochondrial membrane integrity, raising the possibility that point mutations in STARD7 could cause some complex I disorders.

INTRODUCTION

Mitochondrial membranes contain all the major classes of phospholipids found in cell membranes. These include phosphatidic acid (PA), phosphatidylcholine (PC), phosphatidylethanolamine (PE), phosphatidylinositol (PI), and phosphatidylserine (PS). Furthermore, cardiolipin (CL) is a dimeric phospholipid that is found in bacterial and mitochondrial membranes from various organisms. Different phospholipids can assume different orientations in an aqueous milieu based on their overall structure. This has given rise to two major classes of phospholipids: the cylindrical and cone-shaped phospholipids. Cylindrical phospholipids include PC, PI, and PS and are required for forming lipid bilayers. On the other hand, PE, PA, and CL are cone-shaped and impose negative curvatures on membranes, causing membranes to form non-bilayer structures. Thus, specific phospholipids contribute significantly to the integrity of mitochondrial membranes by influencing the physical properties of mitochondrial membranes and through specific protein:phospholipid interactions.[1-3]

Mitochondrial complex I (CI; NADH:ubiquinone oxidoreductase) is the most elaborate component of the oxidative phosphorylation (OXPHOS) system and has an L-shaped structure.[4,5] CI comprises more than 40 subunits in many higher eukaryotes, and we have previously shown that almost all the mammalian CI subunits are conserved in *Drosophila melanogaster* (henceforth referred to as *Dm*; for simplicity, we prefix all *Dm* orthologs of CI subunits with the letter "d" as their exact CG numbers have been described previously).[6-8] There are 14 core subunits that together contain all the catalytic centers of the enzyme and are conserved from the ancestral enzyme in bacteria to the eukaryotic enzyme. The remaining 30 or so subunits are referred to as supernumerary or accessory subunits, as they have no direct bioenergetic functions. It has been hypothesized and proven in some instances that some accessory subunits are involved in maintaining the structural integrity of the enzyme.[9]

Several high-resolution, single-particle cryoelectron microscopy structures (including samples from *Dm*) have shown that the approximately 1 MDa eukaryotic CI has several phospholipid molecules tightly associated with it.[4,5,8,10-12] Most of the CI-associated phospholipids were adjudged to be CL (for those with four acyl side chains), PC, and PE molecules. In the absence of substrates, mammalian CI assumes a dormant state referred to as the de-active state. The de-active state can be reverted to the active state when supplied with NADH and ubiquinone. This active/de-active state transition is relevant physiologically, as ischemia promotes the conversion of CI to the de-active state, an episode hypothesized to protect CI from reactive oxygen species (ROS)-mediated damage.[13,14] Structural data revealed that some phospholipid molecules may regulate transition from the active to the de-active state or vice versa. As an example, two phospholipids that interact with NDUFA9 in mouse CI have been posited to stabilize the loops in ND3 and NDUFA9 that become disordered when the enzyme transitions into the de-active state.[5]

The likely importance of phospholipids in mitochondrial CI bioenergetics is highlighted by the fact that many phospholipids occupy the same locations in CI from different organisms. For instance, the *Yarrowia lipolytica*, mouse, ovine, porcine, and human CI structures have all revealed that many phospholipid molecules are found between the core membrane subunits, especially between the pore-forming, proton-translocating subunits (ND2, ND4, and ND5).[4,5,15-17] Consequently, they may help prevent potential proton leaks during proton translocation from the matrix or help tether various core and accessory membrane subunits together. Other phospholipids appear to have replaced domains or portions of core subunits that are present in bacterial forms of CI but are missing in the mammalian enzyme. These include a CL and three other phospholipids that fill a void left by three ND2 N-terminal helices that have been lost in the mammalian enzyme.[4] Another CL molecule in the ovine enzyme appears to stabilize amphipathic helices at the heel of the boot-shaped complex.[4] In the porcine enzyme, phospholipid molecules stabilize the interactions between the accessory subunit, NDUFA11, and other interacting partners.[16] For instance, a PC molecule is situated between the N terminus of NDUFA11 and the transmembrane helix of NDUFB4; the aliphatic tail of this PC molecule interacts with ND5. Interestingly, a CL and a PE molecule also interact with various segments of NDUFA11. Given that NDUFA11 and NDUFB4 interact with UQCRQ in complex III (CIII) during CI–$CIII_2$ supercomplex formation, the

association of various segments of NDUFA11 and NDUFB4 with phospholipid molecules may influence the stability of the CI–$CIII_2$ supercomplex.

Much has been gleaned from groundbreaking studies in *Saccharomyces cerevisiae* with respect to how disruption of the synthesis of specific phospholipids alters the stability or function of specific OXPHOS complexes or supercomplexes.[18-21] However, because *Saccharomyces cerevisiae* lacks a multi-subunit CI, how various phospholipids influence CI assembly and function has been less characterized. Consequently, we explored the effect of perturbing the mitochondrial membrane phospholipidome on CI assembly in the mitochondria-enriched flight muscles of *Dm*. We find that when the *Dm* ortholog of STARD7 (dSTARD7) is severely disrupted, OXPHOS assembly is impaired and the incorporation of several CI subunits is hampered, as would be expected for a severe perturbation of inner mitochondrial membrane integrity. However, intriguingly, a restrained knockdown of dSTARD7 specifically impairs the incorporation of dNDUFS5 and dNDUFA1 (*Dm* orthologs of NDUFS5 and NDUFA1, respectively) into the proximal part of the protonconducting segment of CI. This is associated with an accumulation of some subcomplexes in the distal part of the membrane domain—most likely a secondary effect to the impaired integration of dNDUFS5 and dNDUFA1 in the membrane domain—as the distal part of the membrane domain can progress in the CI biosynthesis pathway only when all other components of the complex are intact.[6,22-25] Importantly, the restrained knockdown of dSTARD7 appears to induce some amount of CL remodeling, indicating that there could be some degree of alteration in the composition of the mitochondrial phospholipidome. However, a more severe perturbation of CL remodeling via disruption of the CL remodeling enzyme, Tafazzin, does not alter incorporation of dNDUFS5 and dNDUFA1 into CI subcomplexes, which shows that different phospholipid (PL)-modifying enzymes may regulate different aspects of CI biogenesis in the membrane domain.

RESULTS

RNAi-mediated disruption of dSTARD7 in *Dm* flight muscles impairs OXPHOS assembly and activates a compensatory mitochondrial stress response

STARD7, a member of the StAR-related lipid-transfer (START) domain-containing family of lipid transfer proteins, regulates the transport of PC from the outer mitochondrial membrane (OMM) to the inner mitochondrial membrane (IMM) in C2C12 cells[26,27] (Figure 1A). The *Dm* ortholog of STARD7 is CG6565, hereafter referred to as dSTARD7. To interrogate the effect of this protein on CI assembly, we used the Gal4/UAS system[28,29] to express a pair of transgenic RNA interference (RNAi) constructs to dSTARD7 in adult flight muscles using the *Dmef2-Gal4* transgene.[30] Mitochondria from *Dmef2-Gal4/*w^{1118} flies were used as wild-type (WT) controls, as their viability or OXPHOS integrity was indistinguishable from that of mitochondria from *Dmef2-Gal4/UAS-GFP*^{RNA} flies. Western blot analyses of whole-tissue homogenates revealed that the amount of dSTARD7 expressed was significantly attenuated in thoraces from both *Dmef2-Gal4/UAS-dSTARD7*$^{RNAi\text{-}1}$ (dSTARD7-KD1) and *Dmef2-Gal4/UAS-dSTARD7*$^{RNAi\text{-}2}$ (dSTARD7-KD2) flies, relative to *Dmef2-Gal4/*w^{1118} flies (WT) (Figures 1B and S1A-S1C). Analysis of PC levels in an IMM-enriched fraction of mitochondria revealed that PC levels were reduced in samples

from dSTARD7-KD1 thoraces in comparison with samples from WT thoraces (Figure 1C). Interestingly, PC levels were elevated in dSTARD7-KD1 samples when assayed in whole mitochondria fractions, perhaps a reflection of a compensatory response in the OMM to replenish the diminished PC levels in the IMM (Figure 1D). In line with this hypothesis, although the locomotor activity of dSTARD7-KD1 flies was reduced relative to WT flies within the first approximately 96 h after eclosing as adults, it recovered to WT levels around the 144-h time point and was sustained for about 10 days afterward (Figure 1E).

To investigate the effect of disrupting dSTARD7 on the assembly of OXPHOS complexes, we isolated mitochondria from flight muscles of the adult flies 2 days after they emerged as adults, extracted their membranes in digitonin, and examined the integrity of their OXPHOS complexes using blue native polyacrylamide gel electrophoresis (BN-PAGE) and subsequent Coomassie blue staining (Figure 1F).[31-33] Multiple OXPHOS complexes were disrupted in mitochondria from both dSTARD7-KD1 and dSTARD7-KD2 flies (Figure 1F). These results were corroborated with BN-PAGE followed by silver staining of the native gels (Figure 1G). In accord with the Coomassie and silver staining results, in-gel CI, complex II (CII), and complex IV (CIV) activities were reduced in both dSTARD7-KD1 and dSTARD7-KD2 samples (Figures 1H-1J). However, complex V (CV) levels remained relatively unchanged and so essentially served as a loading control.

Mitochondrial stress can increase ROS formation[34]; and in *Dm*, mitochondrial stress can cause an upregulation of immune response genes, chaperones, and antioxidant proteins as part of an intricate adaptive mitochondrial stress signaling cascade.[35-38] Therefore, we examined and detected an increase in ROS formation in thoraces from dSTARD7-KD1 flies 2 days after eclosure (Figures 1K and S1D). To gain further insight into the extent of mitochondrial stress signaling activated 2 days after eclosure under these conditions, we analyzed the expression of a select set of transcripts via quantitative real-time PCR (qPCR) (Figure 1L). We observed a robust induction of several immune-response genes, including *metch* (*mtk*), which was previously used as a reporter for mitochondrial stress (Figure 1L).[35-37] There was some evidence of a mild activation of the JAK-STAT pathway based on the transcriptional induction of the JAK-STAT ligand, *upd2*, and the suppressor of cytokine signaling family gene, *socs36E* (Figure 1L), which is known to be transcriptionally induced by JAK-STAT signaling.[39] Multiple mitochondrial and cytosolic chaperones were also potently upregulated as a result of knocking down dSTARD7 (Figure 1L). However, the effect on antioxidant gene expression was mixed, as several peroxiredoxins (such as *jafrac-1*, CG6888, *prx2540-2*, and *prx6005*) were modestly induced; but superoxide dismutase 1 (*sod1*), superoxide dismutase 2 (*sod2*), catalase (*cat*), and some other peroxiredoxins showed no upregulation at this stage of development (Figure 1L). Similarly, some genes involved in general detoxification, such as the glutathione S-transferases, trended toward induction (Figure 1L). In addition, transcripts of the mtDNA-encoded lrRNA were potently induced as well (Figure 1L). Finally, western blotting showed that there was an upregulation of several proteins involved in regulating the mitochondrial unfolded protein response (Figures S1E and S1F), providing further evidence of an induction of a robust mitochondrial stress signaling network. We note, however, that there were significant disparities between the dSTARD7-KD1 and the dSTARD7-KD2 samples with regard to the extent of induction of several transcripts, perhaps a reflection of a slight difference in extent of dSTARD7

knockdown that was not easy to capture in western blots. Nevertheless, altogether, these observations show that a severe disruption of dSTARD7 impairs the assembly of multiple OXPHOS complexes and activates a compensatory mitochondrial stress response.

Knockdown of dSTARD7 disrupts the biogenesis of several matrix-domain-localized CI subcomplexes

Studies from multiple organisms have long indicated that mitochondrial CI, consisting of matrix and membrane domains, is formed from the amalgamation of three segments of the complex, referred to as the N, Q, and P modules. The N module is the site of NADH oxidation, while the Q module is found between the N module and the membrane domain; the N and Q modules form the matrix domain. The proton-pumping P module is essentially the membrane domain.[7,40,41] Further studies in mammalian systems have revealed that the P module can further be split into proximal and distal parts called the P_P and P_D modules, respectively, and there is growing appreciation among CI biologists that the P_P and P_D modules are found in CI from non-mammalian species as well. As the CI biogenesis pathway has been most characterized in mammalian systems, various groups have defined even more precise models of the CI membrane domain in mammalian systems, such as the ND1, ND2, ND4, and ND5 modules (described by Michael Ryan and colleagues),[42] which are roughly equivalent to the P_P-a, P_P-b, P_D-a, and P_D-b modules, respectively (described by Leo Nijtmans and colleagues).[43] We focused on assessing the impact of dSTARD7 disruption on the definitions of the modules that empirical evidence indicates are conserved in *Dm* (i.e., N, Q, P_P, and P_D modules). Accordingly, we began by exploring the effect of disrupting dSTARD7 on the synthesis of the N and Q modules of CI (Figure 2A).

During CI biogenesis, subcomplexes consisting of a few CI subunits are first synthesized and ultimately merge with other subcomplexes and CI subunits to form the fully assembled complex.[6,40,42] The N, Q, and P modules are synthesized from specific subcomplexes. The Q module consists of dNDUFS2, dNDUFS3, dNDUFS7, dNDUFS8, dNDUFA5, and dNDUFA9. Accordingly, we tracked Q module synthesis by means of immunoblotting of BN gels 2 days after eclosure with antibodies that detect dNDUFS3, dNDUFS7, dNDUFS8, dNDUFA5, and dNDUFA9 (Figures 2B-2F). With the exception of dNDUFA9, where the distribution of subcomplexes was similar between WT and dSTARD7-knockdown samples, all other Q module subunits analyzed revealed a perturbation of at least some of the subcomplexes in the dSTARD7-knockdown samples (Figures 2B-2F). We also monitored N module synthesis by immunoblotting with antibodies that detect dNDUFV1, dNDUFV2, dNDUFV3, dNDUFS4, dNDUFA7, and dNDUFA12 (Figures 2G-2L). The stabilization or incorporation of dNDUFV3 into an initiating subcomplex of the N module was impaired in mitochondria isolated from flight muscles of dSTARD7-KD1 and dSTARD7-KD2 flies, relative to WT (Figure 2G). This was associated with a perturbation in the amount of dNDUFS4 and dNDUFA12 that had incorporated into subcomplexes of the N module (Figures 2H and 2I). However, we did not detect major alterations in the incorporation of dNDUFV1 into subcomplexes (Figure 2J), although at least some dNDUFV2- and dNDUFA7-containing subcomplexes were compromised as well (Figures 2K and 2L). The subcomplex profile observed in the matrix domain as a result of disrupting dSTARD7 expression was reproducible (Figure S2). Altogether, these results indicate that a severe

dSTARD7 disruption impairs the biogenesis or stability of some Q and N module subcomplexes.

Biogenesis of several membrane domain CI subcomplexes is stalled due to disruption of dSTARD7

The membrane domain contains all seven mtDNA-encoded CI subunits (Figure 3A).[7,40,41] To determine the integrity of the membrane domain, we first examined the extent of incorporation of the mtDNA-encoded subunits. We observed a significant decrease in the incorporation or stability of dND1, dND3, dND4L, and dND6 into assembly intermediates (Figures 3B-3E). The results were somewhat complicated for dND2 and dND5, as in both instances there were subcomplexes that appeared unaffected, while others were decreased (for dND2) and increased (for dND5) (Figures 3F and 3G).

We also assessed the extent of incorporation of nuclear-encoded P_P module subunits such as dNDUFS5, dNDUFA8, dNDUFA11, and dNDUFA13 into membrane domain assembly intermediates. The incorporation of dNDUFS5 and dNDUFA8 into the P_P module was impaired in both mutant samples (Figures 3H and 3I). However, incorporation of dNDUFA11 was not appreciably perturbed in a terminal subcomplex in dSTARD7-KD1 flies but showed a robust reduction in dSTARD7-KD2 flies (Figure 3J). Integration of dNDUFA13 into subcomplexes appeared to be only mildly impaired, if at all, as a result of knocking down dSTARD7 (Figure 3K). Therefore, while the exact effect of knocking down dSTARD7 on P_P module subcomplex formation varied, it resulted in the disruption of several subcomplexes.

We also examined the effect of knocking down dSTARD7 expression on the incorporation of P_D module subunits (Figure 3A). In accord with the anti-dND5 immunoblotting data (Figure 3G), immunoblotting against multiple P_D module subunits (i.e., dNDUFB1, dNDUFB5, dNDUFB6, and dNDUFB8) revealed that the P_D module accumulated in both dSTARD7-KD1 and dSTARD7-KD2 samples (Figures 3L-3O). We note that the subcomplex profile observed in the membrane domain as a result of disrupting dSTARD7 expression was reproducible (Figure S3). On the whole, we conclude that disruption of dSTARD7 impairs the biogenesis or leads to a stalling and accumulation of many subcomplexes in the membrane domain. However, the fact that integration of some CI subunits into subcomplexes was normal, and some P_D module subcomplexes accumulated even under these drastic conditions, suggested that CI biogenesis and IMM integrity could be uncoupled.

A restrained knockdown of dSTARD7 preserves mitochondrial membrane integrity

To examine whether the effect of attenuating dSTARD7 expression on CI biogenesis can be uncoupled from dSTARD7's role in regulating IMM integrity, we first explored the effect of a shortened dSTARD7 knockdown period on mitochondrial stress signaling. We reasoned that knocking down dSTARD7 with the potent *Dmef2-Gal4* transgene—which is expressed from the embryonic stage through adulthood—would likely cause a severe disruption of mitochondrial membrane integrity, perhaps causing secondary effects on other PL species, as has been described previously, and make it difficult, if not impossible, to ascertain any direct

effects on CI biogenesis.[19] So we utilized the Demf2-Gal4/UAS system in combination with the tub-Gal80^{ts} system to impair dSTARD7 expression for 5 days, commencing soon after the flies eclosed as adults. The tub-Gal80^{ts} system expresses a temperature-sensitive version of Gal80—which is active at 18°C but relatively inactive at 27°C—ubiquitously.[44] Because Gal80 inhibits Gal4 activity, embryos with the genotype *Dmef2-Gal4; tub-Gal80^{ts}/UAS-dSTARD7^{RNAi-1}* or *Dmef2-Gal4; tub-Gal80^{ts}/UAS-dSTARD7^{RNAi-2}* were grown at 18°C until they reached the adult stage, whereupon they were kept at 27°C for 5 days; *Dmef2-Gal4; tub-Gal80^{ts}/w^{1118}* flies were used as negative controls. Once raised to 27°C, expression of the hitherto dormant RNAi construct commences as a result of the relief of Gal4 inhibition. A modest knockdown effect was observed in the *Dmef2-Gal4; tub-Gal80^{ts}/UAS-dSTARD7^{RNAi-1}* samples after 5 days at 27°C (Figures 4A and 4B). Nevertheless, this was insufficient to cause any OXPHOS assembly defects or an elevation in ROS levels (Figures 4C and 4D). Notably, some degree of mitochondrial stress signaling was present after RNAi-mediated knockdown of dSTARD7 for 5 days at 27°C (Figures 4E, S1G, and S1H); however, the extent of induction of the mitochondrial stress signaling response was far more muted than what was observed in both dSTARD7-KD1 and dSTARD7-KD2 thoraces (Figures 4E, 1L, and S1E-S1H).

The subdued activation of mitochondrial stress signaling in the *Dmef2-Gal4; tub-Gal80^{ts}/UAS-dSTARD7^{RNAi-1}* thoraces caused us to examine whether IMM integrity is intact in mitochondria from these thoraces. To accomplish this task, we analyzed transmission electron micrographs of thoracic sections from adult flies of the following genotypes: (1) *Dmef2-Gal4/w^{1118}*, (2) *Dmef2-Gal4; UAS-dSTARD7*$^{RNAi-1}$, (3) *Dmef2-Gal4; tub-Gal80^{ts}/w^{1118}*, and (4) *Dmef2-Gal4; tub-Gal80^{ts}/UAS-dSTARD7^{RNAi-1}* (Figures 4F-4I). Mitochondria from *Dmef2-Gal4/w^{1118}* flies had the typical well-developed and dense cristae found in normal mitochondria (Figure 4F); but the cristae in mitochondria from *Dmef2-Gal4; UAS-dSTARD7^{RNAi-1}* flies were sparse to nonexistent, and overall mitochondrial quality was compromised (Figure 4G). On the other hand, well-developed and dense cristae were observed in mitochondria from both *Dmef2-Gal4; tub-Gal80^{ts}/w^{1118}* and *Dmef2-Gal4; tub-Gal80^{ts}/UAS-dSTARD7^{RNAi-1}* flies, indicating that the restrained knockdown of dSTARD7 did not impair IMM integrity or crista density (Figures 4H and 4I). Importantly, we uncovered what appeared to be evidence of a modest remodeling of the mitochondrial membrane phospholipidome even at this time point, manifest as alterations in the levels of some PC, PE, and CL species in *Dmef2-Gal4; tub-Gal80^{ts}/UAS-dSTARD7^{RNAi-1}* thoraces relative to *Dmef2-Gal4; tub-Gal80^{ts}/w^{1118}* thoraces (Figure S1I and Table S1). Thus, we conclude that although the paradigm of dSTARD7 knockdown present in *Dmef2-Gal4; tub-Gal80^{ts}/UAS-dSTARD7^{RNAi-1}* flies activates a mild mitochondrial stress response and may cause some degree of alteration of the mitochondrial phospholipidome, it is insufficient to compromise IMM integrity to impede OXPHOS assembly.

Subcomplexes localized to the matrix domain are largely spared as a result of a restrained knockdown of dSTARD7

The preservation of IMM integrity in *Dmef2-Gal4; tub-Gal80^{ts}/UAS-dSTARD7^{RNAi-1}* samples spurred us to explore how a subtle knockdown of dSTARD7 interferes with CI biogenesis independent of its role in maintaining IMM integrity. Accordingly, we analyzed

the distribution of subcomplexes formed in the CI matrix domain of mitochondria from *Dmef2-Gal4; tub-Gal80^{ts}/UAS-dSTARD7^{RNAi-1}* thoraces using antibodies raised against matrix domain subunits (Figure 5A). Matrix domain subcomplexes we detected appeared normal (Figures 5B-5M). We deduce from these results that CI subcomplexes in the matrix domain are largely spared as a result of a restrained knockdown of dSTARD7.

A restrained knockdown of dSTARD7 impedes the biogenesis of some dNDUFS5- and dNDUFA1-containing subcomplexes

We next investigated the effect of a brief attenuation of dSTARD7 expression (restrained knockdown) on the biogenesis of membrane domain subcomplexes (Figure 6A). The mtDNA-encoded subunits were incorporated normally into P_P module subcomplexes (Figures 6B-6F), but we observed a diminished incorporation of dNDUFS5 and dNDUFA1 (Figures 6G, 6H, and S4). None of the other P_P module subunits showed a reproducible incorporation defect into subcomplexes (Figures 6I, 6J, and S5). We conclude that a subtle knockdown of dSTARD7 inhibits the biogenesis of some dNDUFS5- and dNDUFA1-containing subcomplexes.

We also gauged the effect of a mild disruption of dSTARD7 on the incorporation of P_D module subunits. While we did not detect an obstruction in assimilation of most P_D module subunits (Figures 6K-6R and S5), we observed what appeared to be a slight stalling and accumulation of dNDUFB6- and dNDUFB8-containing subcomplexes in the P_D module, indicating that their biogenesis was not impaired (Figures 6O and 6P). Several previous studies from our lab have indicated that the P_D module can progress further in the CI biosynthesis pathway only when all other modules are intact. Consequently, in all previous instances where a genetic manipulation or aging resulted in a perturbation of incorporation of a CI subunit into the Q, N, or P_P module, the P_D module accumulated.[6,22-25] Thus, the minor stalling and accumulation of P_D module subcomplexes is likely a consequence of the inhibition of biogenesis of the dNDUFS5- and dNDUFA1-containing subcomplexes in the P_P module.

Disruption of Tafazzin impairs the biogenesis of a different set of CI subcomplexes

We decided to compare and contrast the restrained knockdown phenotype observed with dSTARD7 with that of another enzyme that can similarly mildly disrupt the biosynthesis of a specific class of mitochondrial PLs. We focused on knocking down Tafazzin, the *Dm* ortholog of TAFAZZIN in humans (also referred to as dTAZ[45]), because dTAZ regulates CL remodeling and has been studied more extensively in *Dm* than other enzymes that regulate PL metabolism. Flies with a mutation in *dTAZ* show reduced locomotor activity, several mitochondrial abnormalities, an 80% reduction in CL, and a diversification of its molecular composition.[45-51]

RNAi-mediated knockdown of *dTAZ* using the *Dmef2-Gal4* transgene mildly disrupted the assembly of multiple OXPHOS complexes (Figure 7A). However, the amount of fully assembled CI detected by immunoblotting of BN gels with more than 20 different CI antibodies was normal when *dTAZ* was knocked down with the *Mhc-Gal4* transgene, which begins to express Gal4 long after *Dmef2-Gal4*, indicating that the IMM was intact (Figures

7B-7I, S1J, S1K, and S6). Further, while integration of most CI subunits into the P module was relatively unimpaired in *Mhc-Gal4/UAS-dTAZ*^{RNAi} flies, assimilation of dNDUFA11, dNDUFB5, and dNDUFB6 was occasionally disrupted, albeit in an inconsistent manner (Figures 7D, 7G, 7H, S6, and S7). Importantly, the incorporation of dNDUFS5 and dNDUFA1 into subcomplexes was not impaired as a result of knocking down the expression of dTAZ (Figures 7C, 7E, and S7). These results, together with those in Figures 5 and 6, indicate that a mild disruption of different enzymes that regulate PL levels in mitochondrial membranes impairs different phases of CI biogenesis in the membrane domain.

DISCUSSION

Studies examining the effects of PL-modifying factors on mitochondrial function in *Dm* have largely focused on dTAZ, due to its effect on CL remodeling.[45-51] However, other PLs also regulate OXPHOS assembly, and when their synthesis is impaired, they can cause mitochondrial disorders. As a case in point, mutations in PS decarboxylase, which converts PS to PE, have been reported to cause mitochondrial disease.[52] By thoroughly defining the mechanism by which all the major PLs in mitochondrial membranes regulate CI function, it might be possible to know *a priori* how different point mutations in regulators of PL synthesis or intramitochondrial PL trafficking alter clinical outcomes of CI disorders.

Accordingly, we explored the role of STARD7 in CI biogenesis. Unlike CL, other mitochondrial PLs are present in the plasma membrane and other organelle membranes as well. Therefore, we chose to analyze IMM PL levels through RNAi-mediated knockdown of dSTARD7. As studies in C2C12 myoblasts have shown that STARD7 largely transports PC from the OMM to the IMM,[26,27] we examined the effect of knocking down dSTARD7 on PC levels. We found that PC levels of an IMM-enriched membrane fraction are reduced, ROS levels are elevated, and OXPHOS assembly is severely impaired when dSTARD7 expression is knocked down by the potent muscle Gal4 transgene, *Dmef2-Gal4*. This is associated with an induction of multiple stress-response genes, ranging from immune-response genes to cytosolic and mitochondrial chaperones, and antioxidant enzymes. The biogenesis of several mitochondrial CI subassemblies and the integrity of the IMM and cristae are severely impaired. Many of these observations are likely a consequence of the severe disruption of mitochondrial membrane integrity as observed in transmission electron micrographs due to a perturbation of PLs in the IMM. Nevertheless, surprisingly, the assimilation of some CI subunits into CI subcomplexes was normal, and some P_D module subcomplexes accumulated even under these austere conditions, hinting at the possibility that CI biogenesis could proceed independent of IMM integrity.

A severe and prolonged disruption of dSTARD7, as is the case when it is knocked down with *Dmef2-Gal4*, would likely cause secondary effects that could mask the initial and direct effects of dSTARD7 disruption. Consequently, in our attempt to circumvent this problem, we used the tub-Gal80^{ts} system to knock down dSTARD7 for 5 days at 27°C after the flies eclosed as adults at 18°C. This resulted in a more restrained and specific phenotype. Although western blots revealed that dSTARD7 expression was reduced, very few of the gene expression changes manifest when dSTARD7 was knocked down with *Dmef2-Gal4* were observed with the Gal80^{ts} system. In addition, with the exception of the

impaired incorporation of dNDUFS5 and dNDUFA1 into P_P module subcomplexes, we did not observe a reproducible diminished incorporation of other CI subunits. This is in contrast to the effect of disrupting dTAZ, which can impair the incorporation of dNDUFA11 and some P_D module subunits into the membrane domain but does not affect the incorporation of dNDUFS5 and dNDUFA1. Interestingly, these results are consistent with the locations of PC and CL in the ovine cryoelectron microscopy (cryo-EM) structure of CI[4]; many of the PC molecules were found in the vicinity of the P_P module, but CL molecules were found in both the P_P and the P_D modules. Importantly, as coenzyme Q prevents oxidative stress, and it has recently been shown that mammalian STARD7 preserves coenzyme Q biosynthesis,[53] we examined whether ROS levels were elevated as a result of the restrained knockdown of dSTARD7. ROS levels were not elevated under the aforementioned conditions, indicating that the results cannot be explained by a deficiency of coenzyme Q. Thus, by impairing the transport of some PLs into the IMM and perhaps remodeling CL, a restrained disruption of STARD7 creates a specialized membrane environment that interferes with the synthesis or stability of assembly intermediates while having essentially no effect on the stability of OXPHOS complexes already made or overall membrane integrity.

Based on these results, it is tempting to speculate on at least one general function of the various PL species interspersed within the membrane domain of CI. The IMM is a very hydrophobic environment, such that all seven core CI subunits in the IMM are encoded on mtDNA and are translated and inserted into the membrane domain almost concurrently. We surmise that there may be situations where a highly hydrophobic accessory subunit is required to promote specific steps in the biogenesis of the P_P and P_D modules; but this cannot be achieved, as all the accessory subunits are nuclear encoded and relatively hydrophilic. In such cases, the mitochondrion solves this problem by using a specific PL species that has the optimal physicochemical properties required to accomplish its purported role. This may also be the reason why the identity and location of many of the PL species are conserved between mouse and ovine CI structures.[4,5]

Accordingly, we postulate that CI-associated PLs have functions analogous to very hydrophobic membrane domain accessory subunits, such that specific PL species inserted in defined crevices of the CI membrane domain engage in specific molecular interactions with neighboring amino acids on some CI subunits, the loss of which impairs incorporation of dNDUFA1 and dNDUFS5 into the P_P module. Therefore, the most definitive experiment to establish their functions would involve obtaining a very high-resolution cryo-EM structure of *Dm* CI that will make it possible to identify any such putative interactions between specific PL species and amino acids. Once such interactions are found, site-directed mutagenesis studies aimed at disrupting the interactions may be needed to definitively confirm their effect on dNDUFA1 and dNDUFS5. We note that an analogous phenomenon has recently been demonstrated for Glu82 in the *Saccharomyces cerevisiae* CIII subunit, Qcr7, which previous structural studies suggested could form hydrogen bonds with the head group of some PE species.[54-56] Notwithstanding these challenges, this study demonstrates that a mild disruption of dSTARD7 can have an impact on the biosynthesis or stability of some CI subcomplexes without affecting the integrity of fully assembled CI and without causing overt changes in mitochondrial membrane integrity.

We note that the muted induction of a mitochondrial stress response could affect the expression levels of other lipid-modifying enzymes localized to the mitochondrion, such as Tafazzin. In this respect, although STARD7 has not been shown to directly regulate CL remodeling, we were able to detect significant remodeling of one CL species 5 days after shifting *Dmef2-Gal4; tub-Gal80^{ts}/UAS-dSTARD7^{RNAi-1}* flies to 27°C, and many other CL species showed a trend of remodeling, although the changes were not deemed statistically significant (Table S1). As PC, which constitutes about half the PL species in mitochondria, is the main source of linoleic acid for CL remodeling in *Dm*,[45] the acyl groups of many PC molecules would likely change as a result. Thus, while the total amount of PC in the IMM may not have changed significantly between WT and mutant dSTARD7 samples, the distribution of various PC species could change. A change in the concentration or composition of both PC and CL would likely lead to compensatory changes in PE, PS, and PI as well. Moreover, we note that even in instances where the changes in PL levels were not adjudged to be statistically significant, this may reflect statistically significant changes within specific crevices of the CI membrane domain of dSTARD7 mutants that, when analyzed in relation to total membrane PLs, are not scored as statistically significant.

Although several PL species are found in mitochondrial membranes, most therapeutic efforts aimed at stabilizing mitochondrial membrane lipids focus on stabilizing CL. This is exemplified by elamipretide—also known as SS-31 or MTP-131—which is a hydrophilic, aromatic-cationic mitochondria-targeting tetrapeptide that localizes to the IMM to stabilize CL and has shown some promise in clinical trialsfor Barth syndrome.[57] Our results indicate that regulating STARD7 expression may be another therapeutic option to pursue in a subset of CI disorders. Notably, STARD7 has been linked to acute asthma,[58] and when STARD7 is disrupted in human or mouse epithelial cells, it impairs mitochondrial homeostasis via a decrease in aerobic respiration, a change in mitochondrial ultra-structure, and an increase in oxidative stress.[59] This is associated with an altered barrier integrity and function. Therefore, our observations are consistent with what has been observed when STARD7 function is impaired in human and mouse epithelial cells and indicate that stabilizing STARD7 might be beneficial to a subset of asthma patients. We note, however, that our results do not preclude additional roles for STARD7 in regulating CI function. For instance, PLs associated with CI have been posited to regulate the active/de-active state transition, reverse electron transport, prevent potential proton leaks during proton translocation through the IMM, and induce conformational changes that have an impact on interactions between coenzyme Q and amino acid residues in the quinone reduction site.[4,5,15-17,60] We anticipate that future studies in *Dm* aimed at thoroughly defining the roles of all PL regulators in bioenergetics will be instrumental in unraveling additional mechanisms by which PLs regulate CI assembly or function *in vivo*.

Limitations of the study

A limitation of this study is our inability to pinpoint the exact PL class (PC, PE, or another PL) or species within a specific class of PLs that directly triggers the phenotypes associated with a restrained knockdown of dSTARD7. Primarily, this is due to a technical limitation arising from the fact that it is virtually impossible to obtain a pure IMM preparation (devoid of any endoplasmic reticulum fragments) to accurately assess IMM PL levels. In addition,

although several reports investigating the function of STARD7 in mammalian systems focus on its role in transporting PC, STARD7 may have the ability to transport PE as well *in vivo*, as it has been shown that disruption of STARD7 in C2C12 cells led to a reduction in both PC and some PE species, such as PE(34:1), in the mitochondrion (see Figure 5 of Horibata et al.[27]). Evidently, further studies are needed to definitively establish the full range of dSTARD7's PL-transporting activities in *Dm*.

STAR★METHODS

RESOURCE AVAILABILITY

Lead contact—Further information and requests for reagents or strains must be directed to and will be fulfilled by the lead contact, Edward Owusu-Ansah (eo2364@cumc.columbia.edu).

Materials availability—Aliquots of some of the antibodies generated will be made available from the lead contact upon reasonable request.

Data and code availability

- All data reported in this paper will be shared by the lead contact upon request. The raw lipidomics data generated during this study are available at MassIVE (UCSD): https://massive.ucsd.edu/ProteoSAFe/dataset.jsp?task=c34af1e0245642b58a0fad75cb35c529 under the deposition number MSV000092254.
- This paper does not report original code.
- Any additional information required to reanalyze the data deposited in this paper is available from the lead contact upon request.

EXPERIMENTAL MODEL AND SUBJECT DETAILS

Drosophila* husbandry—Dm* strains were maintained in vials containing agar, cornmeal medium, molasses and yeast supplemented with propionic acid and methylparaben in humidified environmental chambers (Forma Environmental Chambers, Thermo Fisher Scientific) on a 12-hlight–dark cycle. With the exception of the temperature shift experiments where flies were raised at 18°C or 27°C for the periods indicated in the main text, all other experiments were performed at 25°C. The fly stocks used are described in the Key Resource Table.

METHOD DETAILS

Locomotor activity—Locomotor activity was assessed at 25°C using a *Drosophila* physical activity monitor system (TriKinetics). Specifically, eight adult flies were placed in the *Drosophila* activity monitor and spontaneous movements were recorded continuously for approximately 400 h on a 12-h light–dark cycle.

Purification of mitochondria—Mitochondrial purification was performed essentially as described previously[23-25,32], based on a protocol initially described by Rera et al.[61].

Dissected fly thoraces were gently crushed with a dounce homogenizer in a pre-chilled mitochondrial isolation buffer (MIB; 250 mM sucrose, 0.15 mM $MgCl_2$,10 mM Tris-HCl, pH 7.4) supplemented with Halt Protease Inhibitor Cocktail (Thermo Scientific). Subsequently, the ensuing tissue homogenates were centrifuged twice at 500*g* for 5 min at 4°C to remove the cuticle and other insoluble material. Lastly, the supernatant was recovered and centrifuged at 5000*g* for 5 min at 4°C to obtain the mitochondria-enriched pellet, which was washed twice in the mitochondrial isolation buffer and stored at −80°C until further processing.

Blue native polyacrylamide gel electrophoresis (BN-PAGE)—BN-PAGE was performed as described previously[23-25,32]. Briefly, isolated mitochondria were suspended in NativePAGE sample buffer containing protease inhibitors supplemented with digitonin (MilliporeSigma) at a digitonin:protein ratio of 10:3 , and incubated on ice for 15-20 min prior to centrifugation. Following centrifugation at 20,000*g* for 30 min, the supernatant was recovered, mixed with G-250 sample additive and NativePAGE sample buffer, and loaded onto 3-12% precast Bis-Tris NativePAGE gels. Electrophoreses was performed using the NativePAGE running buffer as anode buffer and the NativePAGE running buffer containing 0.4% Coomassie G-250 as cathode buffer at 4°C. For a set of two gels in the chamber, the operating conditions were 300V and 4mA for approximately 3 h, after which the gels were processed for Coomassie or silver staining as described below. Except where noted, all reagents used herein were from Invitrogen.

Coomassie staining of native gels—Coomassie staining of the gels was performed with the Novex Colloidal Blue Staining Kit (Invitrogen) as follows. The gels were removed from the cassette after electrophoresis, placed in a fixative consisting of 40% methanol and 10% glacial acetic acid and rotated on a shaker for 30 mins. Subsequently, the fixative was replaced with 100 ml of BN-PAGE staining solution (20% methanol, 20% stainer A and 5% stainer B, supplied with the kit) and rotated on a shaker for approximately 16 h (overnight). Afterwards, the staining solution was replaced with 100 ml of a destainer (8% glacial acetic acid) and rotated on the shaker until the bands were visible and background staining was notably reduced. The image was captured with the ChemiDoc Gel Imaging System (Bio-Rad).

Silver staining of native gels—The gels were stained with the SilverXpress Silver Staining Kit (Invitrogen). Briefly, after electrophoresis, the gels were removed from the cassette and placed in a fixative consisting of 40% methanol and 10% glacial acetic acid and rotated on a shaker for at least 10 mins. Afterwards, the fixative was replaced with 100 ml of a sensitizer solution (48% methanol and 2% sensitizer supplied with the kit) and rotated on a shaker for 10 mins. Following sensitization, the gels were washed twice for 5 mins each with 200 ml of ultrapure water. Next, the developer solution supplied with the kit was added and swirled gently until discrete bands appeared with minimal background; at which point the reaction was stopped immediately via addition of the stopper solution supplied with the kit. The image was captured with the ChemiDoc Gel Imaging System .

In-gel complex I, II and IV activity assays—Following the BN-PAGE, the gels were removed from the cassette and subjected to the following procedures: For CI in gel activity, the gel was submerged in a CI in-gel activity assay buffer consisting of 2.5 mg/ml nitrotetrazolium blue chloride, 0.136 mM NADH and 5 mM Tris-HCL (pH 7.4) and rotated on a shaker overnight. For CII in gel activity, the gel was placed in a CII in-gel activity assay solution consisting of 20 mM sodium succinate, 0.2 mM phenazine methosulfate, 2.5 mg/ml nitrotetrazolium blue chloride, and 5 mM Tris-HCL (pH 7.4) and rotated on a shaker overnight. For CIV in gel activity, the gel was placed in a CIV in-gel activity assay buffer comprised of 0.05% 3,3′-diaminobenzidine tetrahydrochloride hydrate, 0.05 mM cytochrome c and 50 mM sodium phosphate (pH 7.2) and rotated on a shaker overnight. In all three instances, the image was captured with a HP LaserJet Scanner.

Amplex red assay for measuring hydrogen peroxide production—The amount of hydrogen peroxide produced was measured with an Amplex Red Hydrogen Peroxide/ Peroxidase Assay Kit (Invitrogen), following the manufacturer's protocol as described previously[24]. In brief, fly thoraces were first homogenized in pre-chilled MIB supplemented with protease inhibitors, after which the homogenate was centrifuged twice at 500*g* for 5 min at 4°C to remove insoluble material. Subsequently, a serial dilution of the supernatant was added to a reaction buffer containing 100 μM Amplex Red reagent and 0.2 U/ml horseradish peroxidase solution. Fluorescence was measured at an excitation wavelength of 540 nm and detected at 590 nm every 30 sec for 30 min at 25°C using a SpectraMax paradigm multi-mode microplate reader (Molecular Devices). The background fluorescence determined for a blank reaction (no H_2O_2) was deducted from each value. Amplex Red activity was normalized to protein concentrations as determined by the Bradford Assay (Bio-Rad) . Samples were analyzed in triplicate.

Phosphatidylcholine assay—The amount of PC in samples was assessed with a Phosphatidylcholine Assay Kit following the manufacturer's instructions (MilliporeSigma, MAK049). Briefly, mitochondria were isolated by homogenizing 200 fly thoraces in MIB containing protease inhibitors. The resulting mitochondrial pellet was split into two portions: one portion was used to determine the concentration of PC from whole mitochondria, while the other portion was used to determine the concentration of PC from a mitochondrial fraction enriched for the IMM. To generate an enriched IMM fraction, mitochondria were incubated with 0.1% digitonin for 10 min on ice to strip off the OMM, followed by centrifugation at 20,000*g* for 10 min. The resulting pellet was enriched for IMM. Both whole mitochondria and IMM-enriched fractions were solubilized in 200 μL of cold PC assay buffer supplied with the kit, and centrifuged at 13,000*g* for 10 min at 4°C to remove insoluble material. A total of 50 μL of the reaction mixture supplied with the kit was added to each standard and experimental sample in a 96-well fluorescence plate, mixed thoroughly, and incubated for 30 min at room temperature protected from light. Fluorescence was measured at an excitation wavelength of 535 nm and detected at 587 nm every 30 sec for 60 min at 25°C using a SpectraMax paradigm multi-mode microplate reader. After normalization of protein concentrations and correcting for background values, the concentration of PC was determined using the PC standard curve and analyzed in triplicate.

Lipidomics—Samples were homogenized in 200 μL of water, suspended in methanol/chloroform (2:1) and incubated at 37°C for 30 minutes to denature proteins. A mixture of internal standards from Avanti Polar Lipids was added consisting of CL standard mix I (303 pmol CL14:1/14:1/14:1/15:1, 277 pmol CL15:0/15:0/15:0/16:1, 254 pmol CL14:1/22:1/22:1/22:1, 231 pmol CL14:1/24:1/24:1/24:1) and Mouse SPLASH (625 pmol PC15:0/18:1d7, 44 pmol PE15:0/18:1d7, 125 pmol PS15:0/18:1d7, 31 pmol PG15:0/18:1d7, 125 pmol PI15:0/18:1d7, 62.5 pmol PA15:0/18:1d7, 281 pmol LPC18:1d7, 12.5 pmol LPE18:1d7, 1562 pmol cholesterol ester18:1d7, 125 pmol plasmenyl-PC18:0/18:1d9, 94 pmol DG15:0/18:1d7, 219 pmol TG15:0/18:1d7/15:0, 125 pmol SMd18:1/18:1d9, 31 pmol plasmenyl-PE18:0/18:1d9). Chloroform and water were added, the samples were vortexed, and phase separation was achieved by centrifugation. The lower phase was collected, dried under nitrogen, and re-dissolved in 200 μL of chloroform/methanol (1:1). Lipids were analyzed by LC-ESI-MS/MS on a Q Exactive HF-X Hybrid Quadrupole-Orbitrap MS System coupled directly to a Vanquish UHPLC (Thermo Fisher Scientific). An aliquot of 5 μl was injected into a Restek Ultra C18 Reversed Phase HPLC Column, 3 μm (Fisher Scientific) that was kept at a temperature of 50°C. Chromatography was performed with solvents A and B at a flow rate of 0.15 mL/min. Solvent A contained 600 ml acetonitrile, 399 ml water, 1 ml formic acid, and 0.631 g ammonium formate. Solvent B contained 900 ml 2-propanol, 99 ml acetonitrile, 1 ml formic acid and 0.631 g ammonium formate. The chromatographic run time was 40 minutes, changing the proportion of solvent B in a non-linear gradient from 30 to 35% (0-2 minutes), from 35 to 67% (2-5 minutes), from 67 to 83% (5-8 minutes), from 83 to 91% (8-11 minutes), from 91 to 95% (11-14 minutes), from 95 to 97% (14-17 minutes), from 97 to 98% (17-20 minutes), from 98 to 100% (20-25 minutes) and from 100 to 30% (25-26 minutes). For the remainder of the run time the proportion of solvent B stayed at 30% (26-40 minutes). To analyze acyl-carnitines, cholesterol esters and glycerides, the mass spectrometer was operated in positive ion mode. For all other lipids, it was operated in negative ion mode. The spray voltage was set to 4 kV and the capillary temperature was set to 350°C. MS1 scans were acquired in profile mode at a resolution of 120,000, an AGC target of 1e6, a maximal injection time of 65 ms and a scan range of 200-2000 m/z. MS2 scans were acquired in profile mode at a resolution of 30,000, an AGC target of 3e6, a maximal injection time of 75 ms, a loop count of 7 and an isolation window of 1.7 m/z. The normalized collision energy was set to 30 and the dynamic exclusion time to 31 s. For lipid identification and quantitation, data were analyzed by the software LipidSearch 5.0 (Thermo Fisher Scientific). The general database was searched with a precursor tolerance of 4 ppm, a product tolerance of 10 ppm, and an intensity threshold of 1.0%.

Transmission electron microscopy—Transmission electron microscopy was performed as described previously[23]. Thoraces were dissected and fixed in a mixture of 2.5% glutaraldehyde and 4% paraformaldehyde in 0.1M cacodylate buffer for 48 h at 4°C and then post-fixed in buffered 1% osmium tetroxide. Samples were subsequently dehydrated in a graded series of acetone and embedded in EMbed 812 resin (Electron Microscopy Sciences). A Leica UC6 ultramicrotome was used to cut 90 nm thin sections which were subsequently stained with a saturated solution of uranyl acetate and lead citrate.

Images were captured with an Advanced Microscopy Techniques XR111 digital camera at 80 kV on a Philips CM12 transmission electron microscope.

Generation of polyclonal antibodies—Rabbit polyclonal antibodies recognizing various segments of specific target proteins in *Drosophila melanogaster* were generated by Biomatik using the synthetic peptides listed below:

Peptide antigen: Cys-GMKYRPGYNADMGDEG Target Protein: dNDUFA10 (CG6343)

Peptide antigen: Cys-PADIIKYVADKEDVYE Target Protein: dNDUFAB1 (CG9160)

Peptide antigen: Cys-GSLSRRKVNSKPEAGR Target Protein: dSTARD7 (CG6565)

Peptide antigen: Cys-RDLRAETEKLHRERN Target Protein: dTAFAZZIN (CG8766)

Immunoblotting—Western blotting was performed as previously described[23-25,32]. Briefly, following the separation of protein complexes on 3–12% precast Bis-Tris NativePAGE gels (Invitrogen), the proteins were transferred to polyvinylidene difluoride (PVDF) membranes (Bio-Rad), by semi-dry transfer using Bio-Rad's Trans-Blot Turbo Transfer System. Subsequently, the PVDF membrane was blocked in 5% (wt/vol) nonfat dry milk (NFDM) in Tris-buffered saline (TBS) for 30 min and incubated in the appropriate primary antibody dissolved in 2% BSA and 0.1% Tween 20 in TBS (TBST) overnight at 4°C. Afterwards, the blot was rinsed four times for 10 min each in 0.1% TBST, blocked for 30 min in 5% (wt/vol) NFDM in TBST, and incubated for 2 h at room temperature with the appropriate HRP-conjugated secondary antibody dissolved in 2% BSA and 0.1% TBST. Following incubation with the secondary antibodies, samples were rinsed four times for 10 min each in 0.1% TBST. Immunoreactivity was detected by a SuperSignal West Pico PLUS Chemiluminescent Kit (Thermo Scientific) and analyzed by a ChemiDoc Gel Imaging System . The primary antibodies used were anti-Actin (MilliporeSigma), anti-ATP synthase, subunit B (Thermo Fisher Scientific), anti-NDUFS3 (Abcam), anti-dNDUFS4[23], anti-dNDUFS5[25], anti-dNDUFS7[24], anti-dNDUFS8[24], anti-dNDUFC2[22], anti-dNDUFV1[25], anti-dNDUFV2[23], anti-dNDUFV3[24], anti-dNDUFA1[22], anti-dNDUFA5[23], anti-dNDUFA6[22], anti-dNDUFA7[23], anti-dNDUFA8[24], anti-dNDUFA9[23], anti-dNDUFA10 (this study) anti-dNDUFA11[24], anti-dNDUFA12[25], anti-dNDUFA13[23], anti-dNDUFAB1 (this study), anti-dNDUFB1[23], anti-dNDUFB2[22], anti-dNDUFB3[22], anti-dNDUFB4[22], anti-dNDUFB5[25], anti-dNDUFB6[25], anti-dNDUFB7[22], anti-dNDUFB8[25], anti-dNDUFB9[22], anti-dNDUFB10[22], anti-dNDUFB11[22], anti-dND1[25], anti-dND2[25], anti-dND3[25], anti-dND4L[25], anti-dND5[25], anti-dND6[25], anti-dTAZ (this study) and anti-dSTARD7 (this study). Secondary antibodies used were goat anti-rabbit horseradish peroxidase (Thermo Fisher Scientific) and goat anti-mouse horseradish peroxidase (Thermo Fisher Scientific).

Quantitative real-time PCR—Quantitative real-time PCR was performed as reported previously[25]. Total RNA was isolated from thoraces using TRIzol Reagent (Thermo Fisher Scientific) and, following the elimination of contaminating DNA, reverse transcribed using the iScript cDNA Synthesis Kit (Bio-Rad). The PCR reaction was performed using Bio-Rad's iQ SYBR Green Supermix. The primers used are listed in Table S2.

QUANTIFICATION AND STATISTICAL ANALYSIS

For statistical analyses and graphical display of data, the GraphPad Prism 9 Software was used. To evaluate whether differences were observed in data from two groups, significance was expressed as *P values* based on the student's *t*-test for unpaired two-tailed samples. For comparisons where two or more experimental groups were compared against a single control group, one-way ANOVA followed by Dunnett's multiple comparisons test was used. The fold change shown in all graphs refers to the mean ± s.e.m (standard error of the mean) and significance was depicted as * for $P<0.05$, ** for $P<0.01$, *** for $P<0.001$ and **** for $P<0.0001$.

Supplementary Material

Refer to Web version on PubMed Central for supplementary material.

ACKNOWLEDGMENTS

We are grateful to many past members of the Owusu-Ansah lab for general discussions. We especially thank Rajesh Patel (Rutgers University) for his assistance with transmission electron microscopy; Yang Xu and Hediye Erdjument-Bromage at New York University for their assistance with depositing the lipidomics raw data files; and Jahar Bhattacharya, Henry Colecraft, Jeanine D'Armiento, Wes Grueber, Laura Johnston, Andrew Marks, Martin Picard, Liza Pon, Eric Schon, and Mimi Shirasu-Hiza at the Columbia University Irving Medical Center for fly stocks, reagents, and general discussions. We acknowledge the Bloomington Drosophila Stock Center, USA; the Fly Stocks of the National Institute of Genetics, Japan; and the Vienna Drosophila Resource Center, Austria, for fly strains.This study was supported by NIH grant GM115593 (R01) to M.S., start-up funds from the Department of Physiology and Cellular Biophysics at the Columbia University Irving Medical Center to E.O.-A., an NIH diversity supplement to E.O.-A. to support M.V., a Provost Junior Faculty Grant to E.O.-A. to support Columbia's diversity efforts, an Irma T. Hirschl Trust Scientist Award to E.O.-A., a Schaeffer Research Scholar Award to E.O.-A., and NIH grants GM124717 (R35) and GM147902 (R01) to E.O.-A.

REFERENCES

1. Horvath SE, and Daum G (2013). Lipids of mitochondria. Prog. Lipid Res 52, 590–614. 10.1016/j.plipres.2013.07.002. [PubMed: 24007978]
2. Ren M, Phoon CKL, and Schlame M (2014). Metabolism and function of mitochondrial cardiolipin. Prog. Lipid Res 55, 1–16. 10.1016/j.plipres.2014.04.001. [PubMed: 24769127]
3. Acoba MG, Senoo N, and Claypool SM (2020). Phospholipid ebb and flow makes mitochondria go. J. Cell Biol 219, e202003131. 10.1083/jcb.202003131. [PubMed: 32614384]
4. Fiedorczuk K, Letts JA, Degliesposti G, Kaszuba K, Skehel M, and Sazanov LA (2016). Atomic structure of the entire mammalian mitochondrial complex I. Nature 538, 406–410. 10.1038/nature19794. [PubMed: 27595392]
5. Agip ANA, Blaza JN, Bridges HR, Viscomi C, Rawson S, Muench SP, and Hirst J (2018). Cryo-EM structures of complex I from mouse heart mitochondria in two biochemically defined states. Nat. Struct. Mol. Biol 25, 548–556. 10.1038/s41594-018-0073-1. [PubMed: 29915388]
6. Garcia CJ, Khajeh J, Coulanges E, Chen EIJ, and Owusu-Ansah E (2017). Regulation of Mitochondrial Complex I Biogenesis in Drosophila Flight Muscles. Cell Rep. 20, 264–278. 10.1016/j.celrep.2017.06.015. [PubMed: 28683319]
7. Rhooms SK, Murari A, Goparaju NSV, Vilanueva M, and Owusu-Ansah E (2020). Insights from Drosophila on mitochondrial complex I. Cell. Mol. Life Sci 77, 607–618. 10.1007/s00018-019-03293-0. [PubMed: 31485716]
8. Padavannil A, Murari A, Rhooms SK, Owusu-Ansah E, and Letts JA (2023). Resting mitochondrial complex I from Drosophila melanogaster adopts a helix-locked state. Elife 12, e84415. 10.7554/eLife.84415. [PubMed: 36952377]

9. Padavannil A, Ayala-Hernandez MG, Castellanos-Silva EA, and Letts JA (2021). The Mysterious Multitude: Structural Perspective on the Accessory Subunits of Respiratory Complex I. Front. Mol. Biosci 8, 798353. 10.3389/fmolb.2021.798353. [PubMed: 35047558]
10. Agip ANA, Blaza JN, Fedor JG, and Hirst J (2019). Mammalian Respiratory Complex I Through the Lens of Cryo-EM. Annu. Rev. Biophys 48, 165–184. 10.1146/annurev-biophys-052118-115704. [PubMed: 30786232]
11. Agip ANA, Chung I, Sanchez-Martinez A, Whitworth AJ, and Hirst J (2023). Cryo-EM structures of mitochondrial respiratory complex I from Drosophila melanogaster. Elife 12, e84424. 10.7554/eLife.84424. [PubMed: 36622099]
12. Parey K, Haapanen O, Sharma V, Köfeler H, Züllig T, Prinz S, Siegmund K, Wittig I, Mills DJ, Vonck J, et al. (2019). High-resolution cryo-EM structures of respiratory complex I: Mechanism, assembly, and disease. Sci. Adv 5, eaax9484. 10.1126/sciadv.aax9484. [PubMed: 31844670]
13. Maklashina E, Sher Y, Zhou HZ, Gray MO, Karliner JS, and Cecchini G (2002). Effect of anoxia/reperfusion on the reversible active/de-active transition of NADH-ubiquinone oxidoreductase (complex I) in rat heart. Biochim. Biophys. Acta 1556, 6–12. 10.1016/s0005-2728(02)00280-3. [PubMed: 12351213]
14. Galkin A, Abramov AY, Frakich N, Duchen MR, and Moncada S (2009). Lack of oxygen deactivates mitochondrial complex I: implications for ischemic injury? J. Biol. Chem 284, 36055–36061. 10.1074/jbc.M109.054346. [PubMed: 19861410]
15. Parey K, Brandt U, Xie H, Mills DJ, Siegmund K, Vonck J, Kühlbrandt W, and Zickermann V (2018). Cryo-EM structure of respiratory complex I at work. Elife 7, e39213. 10.7554/eLife.39213. [PubMed: 30277212]
16. Wu M, Gu J, Guo R, Huang Y, and Yang M (2016). Structure of Mammalian Respiratory Supercomplex I. Cell 167, 1598–1609.e10. 10.1016/j.cell.2016.11.012. [PubMed: 27912063]
17. Guo R, Zong S, Wu M, Gu J, and Yang M (2017). Architecture of Human Mitochondrial Respiratory Megacomplex I. Cell 170, 1247–1257.e12. 10.1016/j.cell.2017.07.050. [PubMed: 28844695]
18. Baker CD, Basu Ball W, Pryce EN, and Gohil VM (2016). Specific requirements of nonbilayer phospholipids in mitochondrial respiratory chain function and formation. Mol. Biol. Cell 27, 2161–2171. 10.1091/mbc.E15-12-0865. [PubMed: 27226479]
19. Calzada E, Avery E, Sam PN, Modak A, Wang C, McCaffery JM, Han X, Alder NN, and Claypool SM (2019). Phosphatidylethanolamine made in the inner mitochondrial membrane is essential for yeast cytochrome bc. Nat. Commun 10, 1432. 10.1038/s41467-019-09425-1. [PubMed: 30926815]
20. Senoo N, Kandasamy S, Ogunbona OB, Baile MG, Lu Y, and Claypool SM (2020). Cardiolipin, conformation, and respiratory complex-dependent oligomerization of the major mitochondrial ADP/ATP carrier in yeast. Sci. Adv 6, eabb0780. 10.1126/sciadv.abb0780. [PubMed: 32923632]
21. Ralph-Epps T, Onu CJ, Vo L, Schmidtke MW, Le A, and Greenberg ML (2021). Studying Lipid-Related Pathophysiology Using the Yeast Model. Front. Physiol 12, 768411. 10.3389/fphys.2021.768411. [PubMed: 34777024]
22. Hossain KFB, Murari A, Mishra B, and Owusu-Ansah E (2022). The membrane domain of respiratory complex I accumulates during muscle aging in Drosophila melanogaster. Sci. Rep 12, 22433. 10.1038/s41598-022-26414-5. [PubMed: 36575244]
23. Murari A, Goparaju NSV, Rhooms SK, Hossain KFB, Liang FG, Garcia CJ, Osei C, Liu T, Li H, Kitsis RN, et al. (2022). IDH2-mediated regulation of the biogenesis of the oxidative phosphorylation system. Sci. Adv 8, eabl8716. 10.1126/sciadv.abl8716. [PubMed: 35544578]
24. Murari A, Rhooms SK, Garcia C, Liu T, Li H, Mishra B, Deshong C, and Owusu-Ansah E (2021). Dissecting the concordant and disparate roles of NDUFAF3 and NDUFAF4 in mitochondrial complex I biogenesis. iScience 24, 102869. 10.1016/j.isci.2021.102869. [PubMed: 34386730]
25. Murari A, Rhooms SK, Goparaju NS, Villanueva M, and Owusu-Ansah E (2020). An antibody toolbox to track complex I assembly defines AIF's mitochondrial function. J. Cell Biol 219, e202001071. 10.1083/jcb.202001071. [PubMed: 32936885]
26. Horibata Y, Ando H, Zhang P, Vergnes L, Aoyama C, Itoh M, Reue K, and Sugimoto H (2016). StarD7 Protein Deficiency Adversely Affects the Phosphatidylcholine Composition, Respiratory

Activity, and Cristae Structure of Mitochondria. J. Biol. Chem 291, 24880–24891. 10.1074/jbc.M116.736793. [PubMed: 27694445]

27. Horibata Y, Mitsuhashi S, Shimizu H, Maejima S, Sakamoto H, Aoyama C, Ando H, and Sugimoto H (2020). The phosphatidylcholine transfer protein StarD7 is important for myogenic differentiation in mouse myoblast C2C12 cells and human primary skeletal myoblasts. Sci. Rep 10, 2845. 10.1038/s41598-020-59444-y. [PubMed: 32071354]
28. Fischer JA, Giniger E, Maniatis T, and Ptashne M (1988). GAL4 activates transcription in Drosophila. Nature 332, 853–856. 10.1038/332853a0. [PubMed: 3128741]
29. Brand AH, and Perrimon N (1993). Targeted gene expression as a means of altering cell fates and generating dominant phenotypes. Development 118, 401–415. 10.1242/dev.118.2.401. [PubMed: 8223268]
30. Ranganayakulu G, Schulz RA, and Olson EN (1996). Wingless signaling induces nautilus expression in the ventral mesoderm of the Drosophila embryo. Dev. Biol 176, 143–148. 10.1006/dbio.1996.9987. [PubMed: 8654890]
31. Fernandez-Vizarra E, and Zeviani M (2021). Blue-Native Electrophoresis to Study the OXPHOS Complexes. Methods Mol. Biol 2192, 287–311. 10.1007/978-1-0716-0834-0_20. [PubMed: 33230780]
32. Murari A, and Owusu-Ansah E (2021). Analyzing the integrity of oxidative phosphorylation complexes in Drosophila flight muscles. STAR Protoc. 2, 101021. 10.1016/j.xpro.2021.101021. [PubMed: 34977670]
33. Jha P, Wang X, and Auwerx J (2016). Analysis of Mitochondrial Respiratory Chain Supercomplexes Using Blue Native Polyacrylamide Gel Electrophoresis (BN-PAGE). Curr. Protoc. Mouse Biol 6, 1–14. 10.1002/9780470942390.mo150182. [PubMed: 26928661]
34. Hernansanz-Agustín P, and Enríquez JA (2021). Generation of Reactive Oxygen Species by Mitochondria. Antioxidants 10, 415. 10.3390/antiox10030415. [PubMed: 33803273]
35. Borch Jensen M, Qi Y, Riley R, Rabkina L, and Jasper H (2017). PGAM5 promotes lasting FoxO activation after developmental mitochondrial stress and extends lifespan in. Elife 6, e26952. 10.7554/eLife.26952. [PubMed: 28891792]
36. Owusu-Ansah E, Song W, and Perrimon N (2013). Muscle mitohormesis promotes longevity via systemic repression of insulin signaling. Cell 155, 699–712. 10.1016/j.cell.2013.09.021. [PubMed: 24243023]
37. Owusu-Ansah E, and Banerjee U (2009). Reactive oxygen species prime Drosophila haematopoietic progenitors for differentiation. Nature 461, 537–541. 10.1038/nature08313. [PubMed: 19727075]
38. Owusu-Ansah E, Yavari A, Mandal S, and Banerjee U (2008). Distinct mitochondrial retrograde signals control the G1-S cell cycle checkpoint. Nat. Genet 40, 356–361. 10.1038/ng.2007.50. [PubMed: 18246068]
39. Karsten P, Häder S, and Zeidler MP (2002). Cloning and expression of Drosophila SOCS36E and its potential regulation by the JAK/STAT pathway. Mech. Dev 117, 343–346. 10.1016/s0925-4773(02)00216-2. [PubMed: 12204282]
40. Formosa LE, Dibley MG, Stroud DA, and Ryan MT (2018). Building a complex complex: Assembly of mitochondrial respiratory chain complex I. Semin. Cell Dev. Biol 76, 154–162. 10.1016/j.semcdb.2017.08.011. [PubMed: 28797839]
41. Vartak RS, Semwal MK, and Bai Y (2014). An update on complex I assembly: the assembly of players. J. Bioenerg. Biomembr 46, 323–328. 10.1007/s10863-014-9564-x. [PubMed: 25030182]
42. Stroud DA, Surgenor EE, Formosa LE, Reljic B, Frazier AE, Dibley MG, Osellame LD, Stait T, Beilharz TH, Thorburn DR, et al. (2016). Accessory subunits are integral for assembly and function of human mitochondrial complex I. Nature 538, 123–126. 10.1038/nature19754. [PubMed: 27626371]
43. Guerrero-Castillo S, Baertling F, Kownatzki D, Wessels HJ, Arnold S, Brandt U, and Nijtmans L (2017). The Assembly Pathway of Mitochondrial Respiratory Chain Complex I. Cell Metab. 25, 128–139. 10.1016/j.cmet.2016.09.002. [PubMed: 27720676]
44. McGuire SE, Mao Z, and Davis RL (2004). Spatiotemporal gene expression targeting with the TARGET and gene-switch systems in Drosophila. Sci. STKE 2004. 10.1126/stke.2202004pl6.

45. Xu Y, Malhotra A, Ren M, and Schlame M (2006).The enzymatic function of tafazzin. J. Biol. Chem 281, 39217–39224. 10.1074/jbc.M606100200. [PubMed: 17082194]
46. Xu Y, Condell M, Plesken H, Edelman-Novemsky I, Ma J, Ren M, and Schlame M (2006). A Drosophila model of Barth syndrome. Proc. Natl. Acad. Sci. USA 103, 11584–11588. 10.1073/pnas.0603242103. [PubMed: 16855048]
47. Xu Y, Anjaneyulu M, Donelian A, Yu W, Greenberg ML, Ren M, Owusu-Ansah E, and Schlame M (2019). Assembly of the complexes of oxidative phosphorylation triggers the remodeling of cardiolipin. Proc. Natl. Acad. Sci. USA 116, 11235–11240. 10.1073/pnas.1900890116. [PubMed: 31110016]
48. Damschroder D, Reynolds C, and Wessells R (2018). Drosophila tafazzin mutants have impaired exercise capacity. Physiol. Rep 6, e13604. 10.14814/phy2.13604. [PubMed: 29405656]
49. Xu Y, Malhotra A, Claypool SM, Ren M, and Schlame M (2015). Tafazzins from Drosophila and mammalian cells assemble in large protein complexes with a short half-life. Mitochondrion 21, 27–32. 10.1016/j.mito.2015.01.002. [PubMed: 25598000]
50. Schlame M, Blais S, Edelman-Novemsky I, Xu Y, Montecillo F, Phoon CKL, Ren M, and Neubert TA (2012). Comparison of cardiolipins from Drosophila strains with mutations in putative remodeling enzymes. Chem. Phys. Lipids 165, 512–519. 10.1016/j.chemphyslip.2012.03.001. [PubMed: 22465155]
51. Xu Y, Zhang S, Malhotra A, Edelman-Novemsky I, Ma J, Kruppa A, Cernicica C, Blais S, Neubert TA, Ren M, and Schlame M (2009). Characterization of tafazzin splice variants from humans and fruit flies. J. Biol. Chem 284, 29230–29239. 10.1074/jbc.M109.016642. [PubMed: 19700766]
52. Zhao T, Goedhart CM, Sam PN, Sabouny R, Lingrell S, Cornish AJ, Lamont RE, Bernier FP, Sinasac D, Parboosingh JS, et al. (2019). *PISD* is a mitochondrial disease gene causing skeletal dysplasia, cataracts, and white matter changes. Life Sci. Alliance 2, e201900353. 10.26508/lsa.201900353. [PubMed: 30858161]
53. Deshwal S, Onishi M, Tatsuta T, Bartsch T, Cors E, Ried K, Lemke K, Nolte H, Giavalisco P, and Langer T (2023). Mitochondria regulate intracellular coenzyme Q transport and ferroptotic resistance via STARD7. Nat. Cell Biol 25, 246–257. 10.1038/s41556-022-01071-y. [PubMed: 36658222]
54. Wenz T, Hielscher R, Hellwig P, Schägger H, Richers S, and Hunte C (2009). Role of phospholipids in respiratory cytochrome bc(1) complex catalysis and supercomplex formation. Biochim. Biophys. Acta 1787, 609–616. 10.1016/j.bbabio.2009.02.012. [PubMed: 19254687]
55. Lange C, Nett JH, Trumpower BL, and Hunte C (2001). Specific roles of protein-phospholipid interactions in the yeast cytochrome bc1 complex structure. EMBO J. 20, 6591–6600. 10.1093/emboj/20.23.6591. [PubMed: 11726495]
56. Calzada E, Avery E, Sam PN, Modak A, Wang C, McCaffery JM, Han X, Alder NN, and Claypool SM (2019). Phosphatidylethanolamine made in the inner mitochondrial membrane is essential for yeast cytochrome bc(1) complex function. Nat. Commun 10, 1432. 10.1038/s41467-019-09425-1. [PubMed: 30926815]
57. Sabbah HN (2021). Barth syndrome cardiomyopathy: targeting the mitochondria with elamipretide. Heart Fail. Rev 26, 237–253. 10.1007/s10741-020-10031-3. [PubMed: 33001359]
58. Yang L, Lewkowich I, Apsley K, Fritz JM, Wills-Karp M, and Weaver TE (2015). Haploinsufficiency for Stard7 is associated with enhanced allergic responses in lung and skin. J. Immunol 194, 5635–5643. 10.4049/jimmunol.1500231. [PubMed: 25980009]
59. Yang L, Na CL, Luo S, Wu D, Hogan S, Huang T, and Weaver TE (2017). The Phosphatidylcholine Transfer Protein Stard7 is Required for Mitochondrial and Epithelial Cell Homeostasis. Sci. Rep 7, 46416. 10.1038/srep46416. [PubMed: 28401922]
60. Jussupow A, Di Luca A, and Kaila VRI (2019). How cardiolipin modulates the dynamics of respiratory complex I. Sci. Adv 5, eaav1850. 10.1126/sciadv.aav1850. [PubMed: 30906865]
61. Rera M, Bahadorani S, Cho J, Koehler CL, Ulgherait M, Hur JH, Ansari WS, Lo T, Jones DL, and Walker DW (2011). Modulation of longevity and tissue homeostasis by the Drosophila PGC-1 homolog. Cell Metab. 14, 623–634. 10.1016/j.cmet.2011.09.013. [PubMed: 22055505]

Highlights

- The *Drosophila melanogaster* ortholog of STARD7 (CG6565) regulates OXPHOS assembly
- STARD7 can regulate membrane integrity and OXPHOS assembly independently
- A restrained knockdown of STARD7 impairs biogenesis of the P_P module of complex I
- STARD7 regulates the biogenesis of some NDUFS5- and NDUFA1-containing subcomplexes

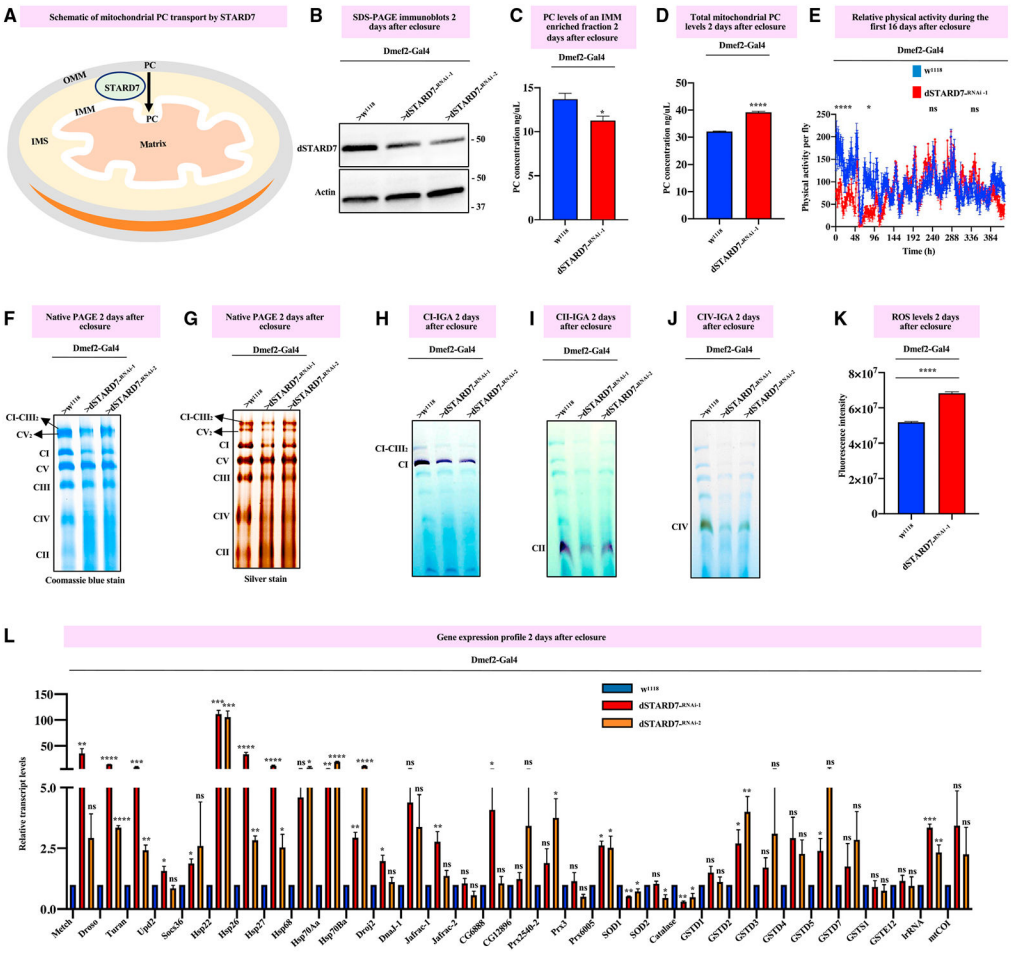

Figure 1. RNAi-mediated disruption of dSTARD7 in *Drosophila* flight muscles impairs OXPHOS assembly and activates a compensatory mitochondrial stress response

(A) A schematic describing the role of STARD7 in transporting PC from the OMM to the IMM.

(B) Total tissue lysates from flight/thoracic muscles isolated from *Dmef2-Gal4/UAS-dSTARD7*$^{RNAi-1}$ (dSTARD7-KD1) and *Dmef2-Gal4/UAS-dSTARD7*$^{RNAi-2}$(dSTARD7-KD2) flies, relative to *Dmef2-Gal4/w*^{1118} flies (wild type, WT) were analyzed by SDS-PAGE and immunoblotting with anti-dSTARD7 and anti-actin antibodies. The flies were dissected 2 days after they eclosed as adults, and the expression level of actin was used as a loading control.

(C and D) Relative PC levels of an IMM-enriched fraction of mitochondria (C) and a whole mitochondria fraction (D) isolated from thoraces of flies with the genotypes shown 2 days after they eclosed as adults.

(E) Relative spontaneous physical activities of dSTARD7-KD1 and WT flies during the first 16 days after eclosure.

(F–J) Mitochondrial preparations from dSTARD7-KD1, dSTARD7-KD2, and WT thoraces 2 days after eclosure were analyzed by Coomassie staining of blue native polyacrylamide gels (F), silver staining of blue native polyacrylamide gels (G), and CI, CII, and CIV in-gel activity (IGA) assays (H–J).

(K) Relative ROS levels of whole-tissue homogenates isolated from flight muscles with the genotypes shown 2 days after the flies eclosed as adults. ROS levels were measured with an Amplex Red Hydrogen Peroxide/Peroxidase Assay Kit.

(L) Relative levels of expression of various mitochondrial stress-response genes in thoraces of dSTARD7-KD1 and dSTARD7-KD2 flies, relative to WT thoraces. Relative transcript levels were analyzed by qPCR.

In (C)–(E) and (K), p values are based on Student's t test for unpaired two-tailed samples. One-way ANOVA followed by Dunnett's multiple comparisons test was used to compute p values in (L). The fold change shown refers to the mean ± SEM (standard error of the mean); ns, $p > 0.05$; *$p < 0.05$, **$p < 0.01$, ***$p < 0.001$, and ****$p < 0.0001$. The number of replicates (n) = 3 biological replicates, with 100 flies per replicate in (C) and (D) and 10 flies per replicate in (K) and (L). In (E), n = 8 flies.

See Figure S1 for replicates and quantification of immunoblots and ROS levels.

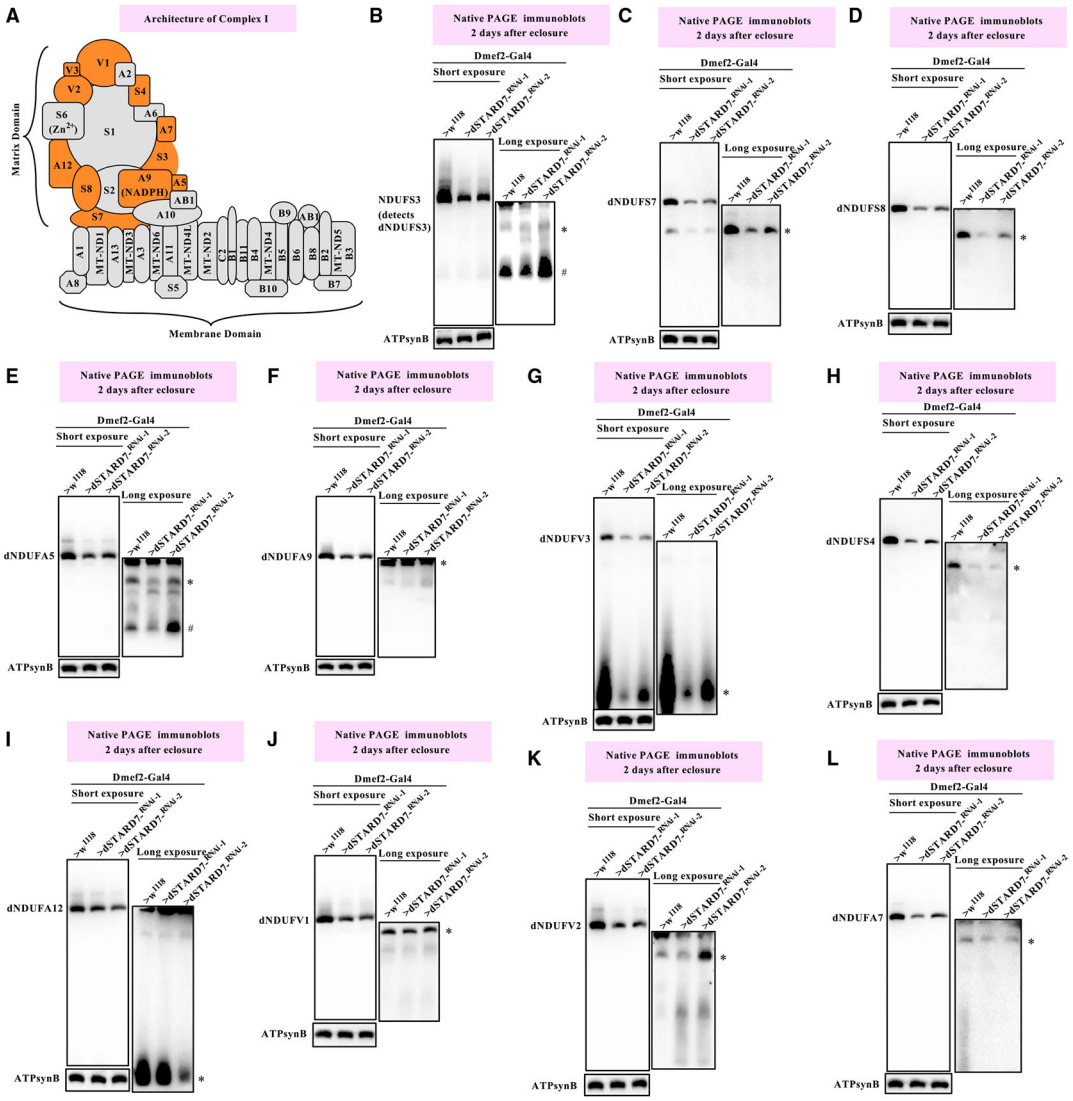

Figure 2. Knockdown of dSTARD7 disrupts the biogenesis of several matrix-domain-localized CI subcomplexes

(A) A representation of mitochondrial CI depicting the relative positions of its multiple subunits based on recent cryo-EM studies on the structure of CI in *Dm*[8,11] and with the subunits analyzed by immunoblotting in (B)–(L) highlighted in orange. The first three letters in the names of the CI subunits have been omitted for brevity. N module biogenesis was monitored by immunoblotting with antibodies we raised against dNDUFV1, dNDUFV2, dNDUFV3, dNDUFS4, dNDUFA7, and dNDUFA12. A commercially available antibody that detects dNDUFS3 and antibodies we generated against dNDUFS7, dNDUFS8, dNDUFA5, and dNDUFA9 were used to assess the biogenesis of the Q module.

(B–L) Mitochondrial preparations from thoraces dissected from dSTARD7-KD1, dSTARD7-KD2, and WT flies 2 days after eclosure were analyzed by BN-PAGE, followed by immunoblotting with the antibodies indicated. Polyvinylidene difluoride (PVDF) membranes were imaged following a short exposure to detect the holoenzyme and supercomplexes, after which the region corresponding to the holoenzyme and

supercomplexes was cut off and the rest of the blot re-imaged after a longer exposure to detect the subcomplexes or assembly intermediates. Antibodies used were anti-NDUFS3, which detects dNDUFS3 (B), anti-dNDUFS7 (C), anti-dNDUFS8 (D), anti-dNDUFA5 (E), anti-dNDUFA9 (F), anti-dNDUFV3 (G), anti-dNDUFS4 (H), anti-dNDUFA12 (I), anti-dNDUFV1 (J), anti-dNDUFV2 (K), and anti-dNDUFA7 (L). Anti-ATP synthase, subunit B (ATP5F1B), which detects the *Drosophila* ortholog, ATPsynB, was used as a loading control in all figures involving immunoblots of blue native gels in this article. The symbol # refers to the initiating subcomplex or assembly intermediate of the Q module; other subcomplexes are denoted as *. See Figure S2 for replicates and quantification of immunoblots.

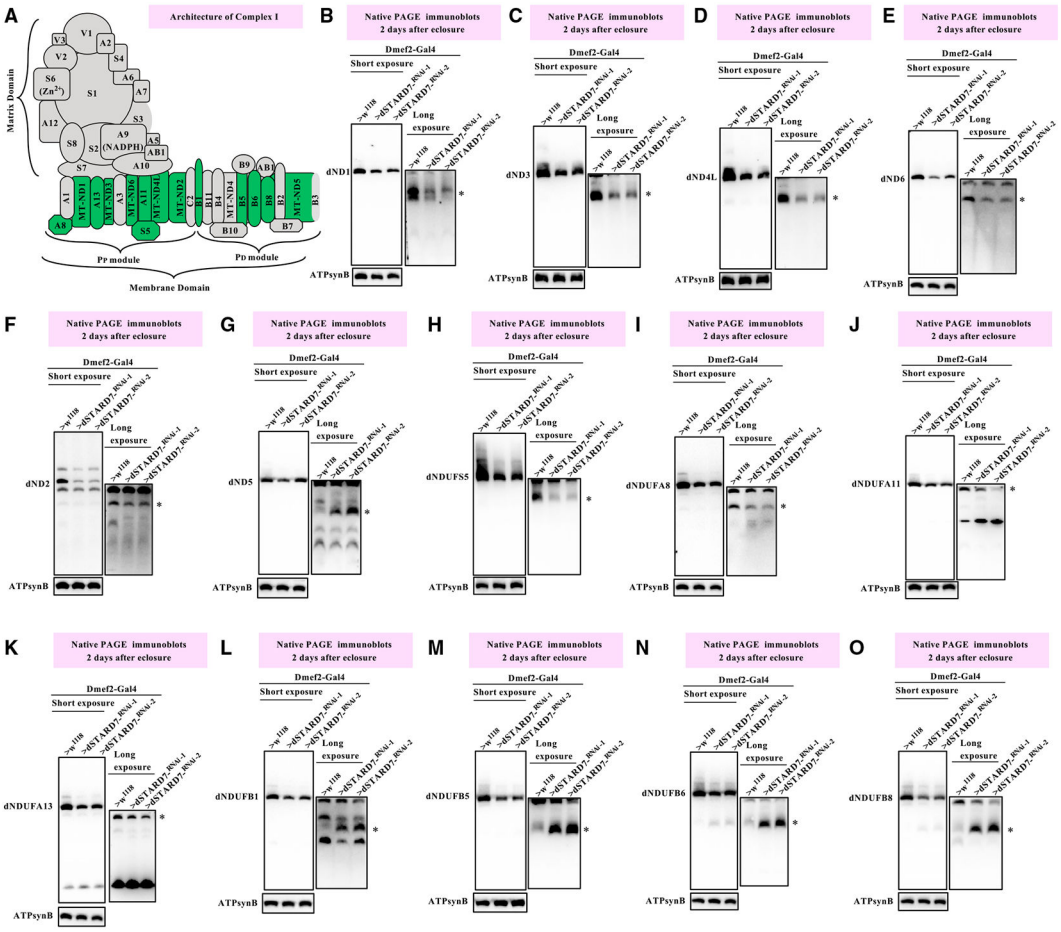

Figure 3. Biogenesis of several membrane domain CI subcomplexes is stalled due to disruption of dSTARD7

(A) An illustration of CI and the antibodies to subunits used to probe the synthesis of the P_P and P_D modules of the membrane domain, shown in green.

(B–O) Mitochondrial preparations from flight muscles isolated from flies 2 days after eclosure and with the genotypes indicated were analyzed by BN-PAGE, followed by immunoblotting with the antibodies listed. The antibodies used were anti-dND1 (B), anti-dND3 (C), anti-dND4L (D), anti-dND6 (E), anti-dND2 (F), anti-dND5 (G), anti-dNDUFS5 (H), anti-dNDUFA8 (I), anti-dNDUFA11 (J), anti-dNDUFA13 (K), anti-dNDUFB1 (L), anti-dNDUFB5 (M), anti-dNDUFB6 (N) and anti-dNDUFB8 (O). Subcomplexes that were quantified are denoted as *. See Figure S3 for replicates and quantification of immunoblots.

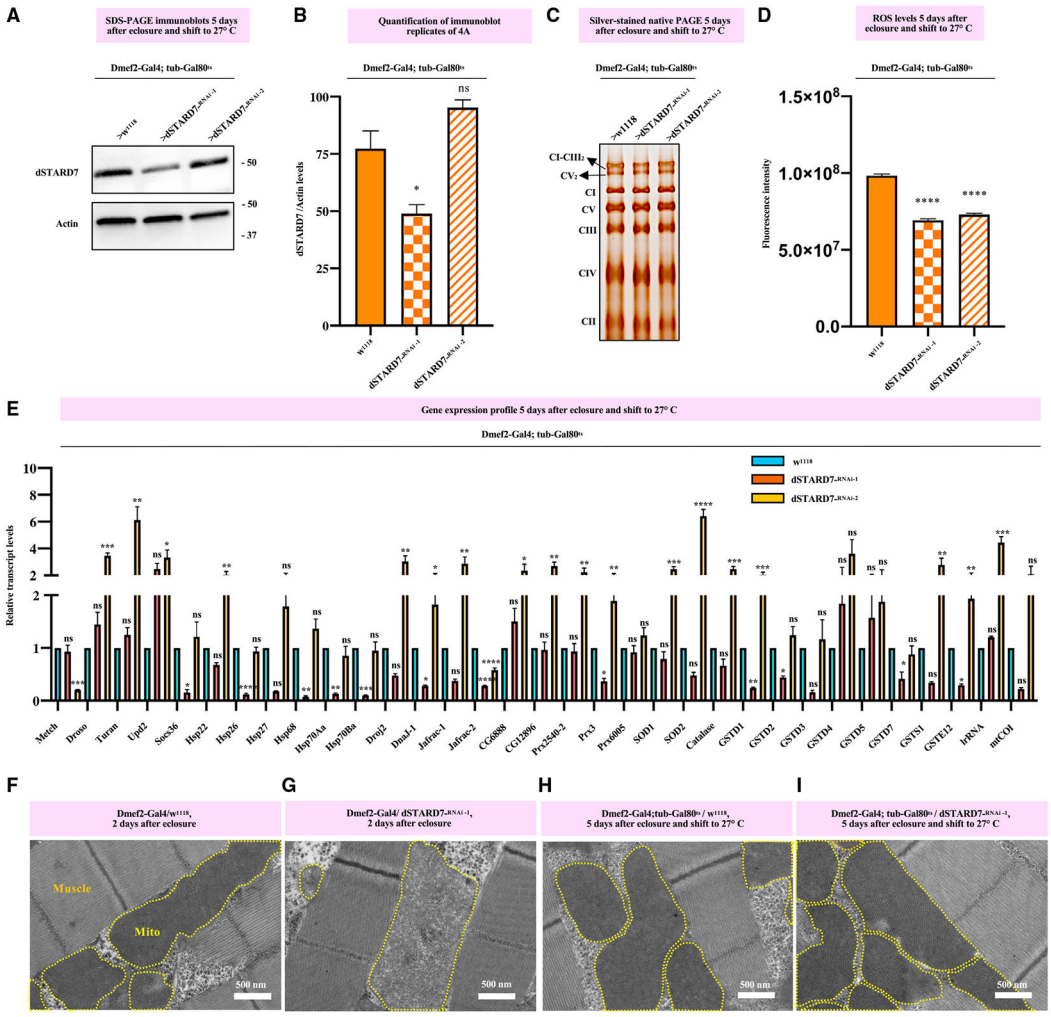

Figure 4. A restrained knockdown of dSTARD7 preserves mitochondrial membrane integrity

(A) Anti-dSTARD7 and anti-actin immunoblotting of total tissue lysates of thoracic muscles obtained from flies raised at 18°C until they reached the adult stage, whereupon they were kept at 27°C for 5 days. The expression level of actin was used as a loading control.

(B) Quantification of replicates of immunoblots described in (A).

(C) Mitochondrial preparations from adult flight muscles of flies with the genotypes indicated were analyzed by silver staining of blue native polyacrylamide gels 5 days after the shift to 27° C.

(D) Relative ROS levels of whole-tissue homogenates isolated from flight muscles with the genotypes shown 5 days after the shift to 27° C.

(E) Relative gene expression levels of some mitochondrial stress-response genes in thoraces of flies with the genotypes shown assessed by qPCR.

(F–I) Transmission electron micrographs (TEMs) of flight muscle sections from WT (F), dSTARD7-KD1 (G), *Dmef2-Gal4; tub-Gal80^{ts}/w^{1118}* (H), and *Dmef2-Gal4; tub-Gal80^{ts}/ UAS-dSTARD7^{RNAi-1}* (I) flies dissected at the indicated time points. Scale bars are as shown, and the dotted yellow lines demarcate the mitochondria. One-way ANOVA followed by Dunnett's multiple comparisons test was used to compute p values in (B), (D), and (E).

The fold change shown refers to the mean ± SEM (standard error of the mean); ns, $p > 0.05$; *$p < 0.05$, **$p < 0.01$, ***$p < 0.001$, and ****$p < 0.0001$. The number of replicates (n) = 3 biological replicates, with 10 flies per replicate. Also, see Figure S1.

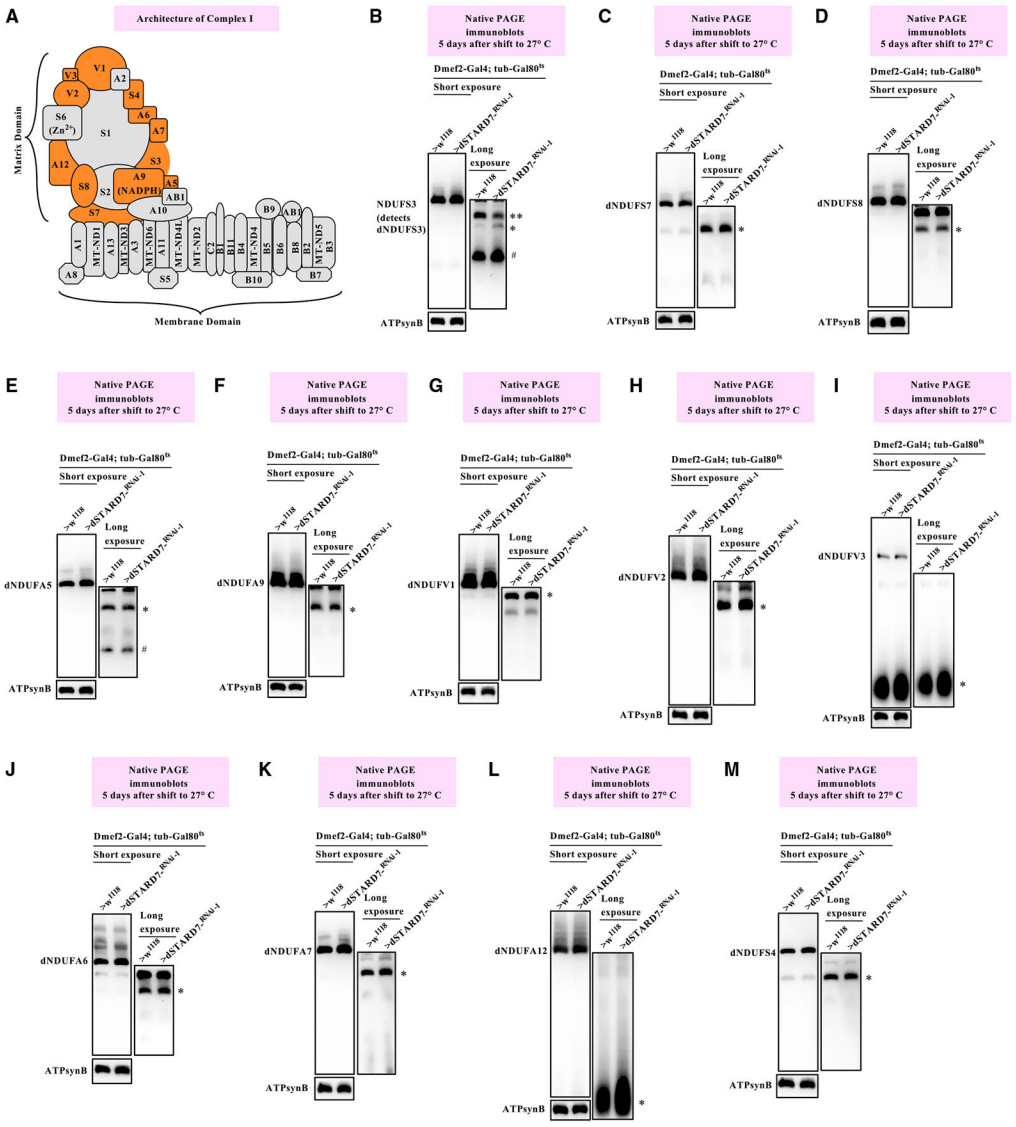

Figure 5. Subcomplexes localized to the matrix domain are largely spared as a result of a restrained knockdown of dSTARD7

(A) A representation of CI depicting the antibodies used to track the biogenesis of the N and Q modules in the matrix domain.

(B–M) BN-PAGE followed by immunoblotting with the antibodies listed. The antibodies used were as follows: anti-NDUFS3, which detects dNDUFS3 (B), anti-dNDUFS7 (C), anti-dNDUFS8 (D), anti-dNDUFA5 (E), anti-dNDUFA9 (F), anti-dNDUFV1 (G), anti-dNDUFV2 (H), anti-dNDUFV3 (I), anti-dNDUFA6 (J), anti-dNDUFA7 (K), anti-dNDUFA12 (L), and anti-dNDUFS4 (M). Subcomplexes denoted with #, *, and ** were quantified. Also, see Figure S4.

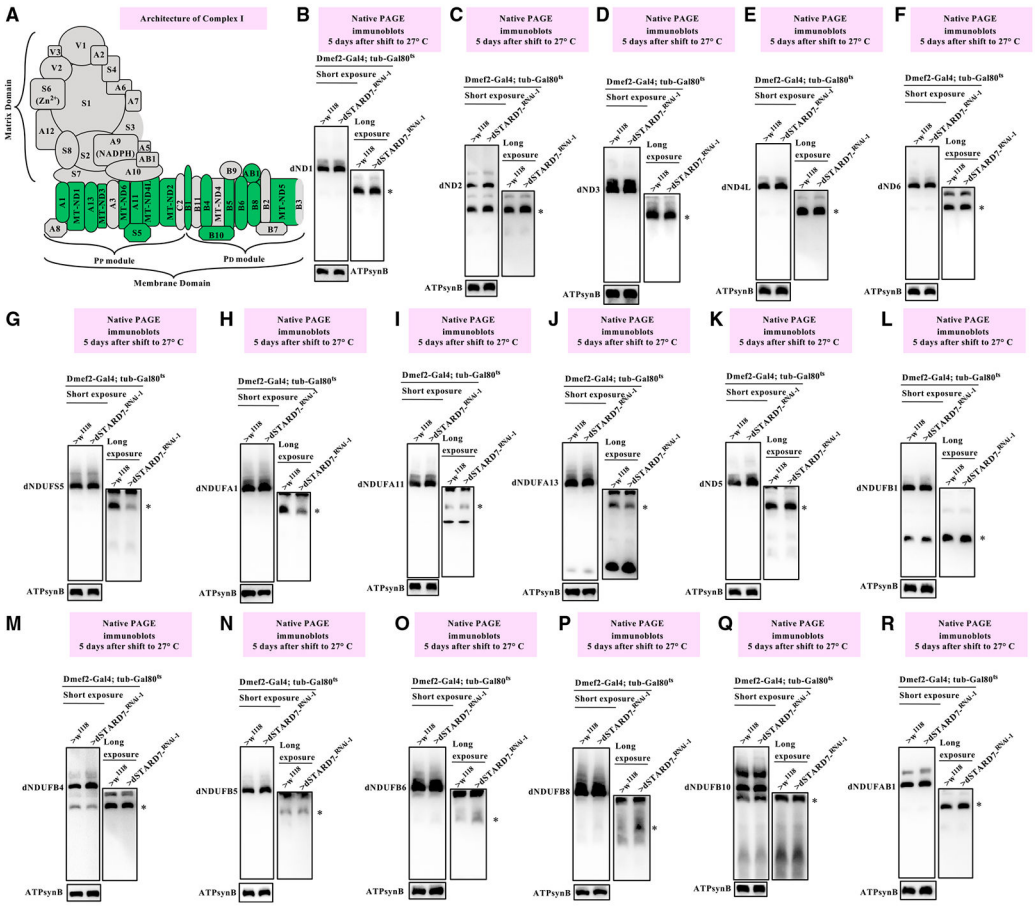

Figure 6. A restrained knockdown of dSTARD7 impedes the biogenesis of some dNDUFS5- and dNDUFA1-containing subcomplexes

(A) An illustration of CI and the antibodies used to monitor the synthesis of subcomplexes in the membrane domain.

(B–R) The antibodies used to monitor biogenesis of the P_P and P_D modules of the membrane domain are as indicated. Subcomplexes that were analyzed are denoted as *. Also, see Figure S4 and S5.

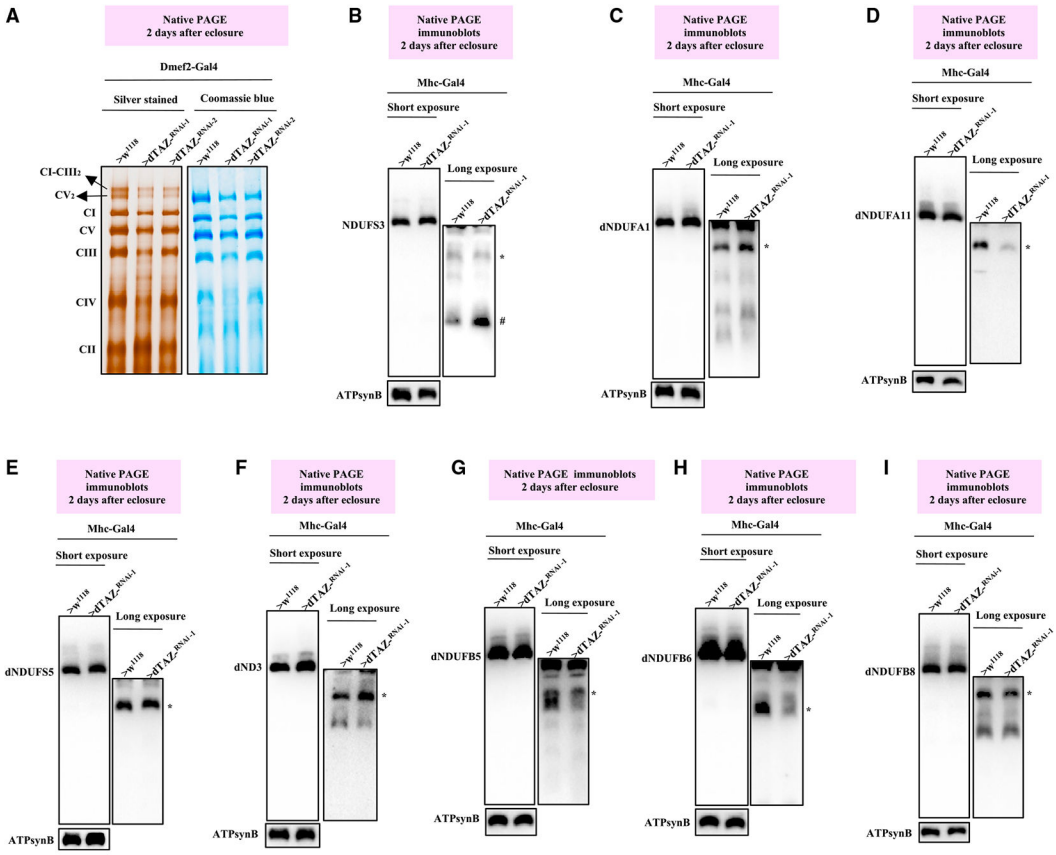

Figure 7. Disruption of Tafazzin impairs the biogenesis of a different set of CI subcomplexes

(A) Mitochondrial preparations from adult flight muscles of flies with the genotypes indicated were analyzed by silver staining (left) or Coomassie blue staining (right) of blue native polyacrylamide gels 2 days after eclosing as adults.

(B–I) Antibodies used to track biogenesis of the various CI subcomplexes are as specified. Subcomplexes that were analyzed are denoted as # or *. Also, see Figure S6 for immunoblotting with additional antibodies and Figure S7 for replicates and quantification of western blots shown here.

KEY RESOURCES TABLE

REAGENT or RESOURCE	SOURCE	IDENTIFIER
Antibodies		
Mouse anti-NDUFS3	Abcam	Cat #: ab14711; RRID: AB_301429
Mouse anti-ATPsynß	Thermo Fisher Scientific	Cat #: A-21351; RRID: AB_221512
Rabbit anti-Hsp60 (D307)	Cell Signaling Technology	Cat #: 4870S; RRID: AB_2295614
Mouse anti-Actin	MilliporeSigma	Cat #: MAB-1501; RRID: AB_2223041
Goat anti-rabbit HRP	Thermo Fisher Scientific	Cat #: 31460; RRID: AB_228341
Goat anti-mouse HRP	Thermo Fisher Scientific	Cat #: 31430; RRID: AB_228307
Rabbit anti-dNDUFA1 (CG34439)	(Hossain et al., 2022)[22]	NA
Rabbit anti-dNDUFA5 (CG6463)	(Murari et al., 2022)[23]	NA
Rabbit anti-dNDUFA6 (CG7712)	(Hossain et al., 2022)[22]	NA
Rabbit anti-dNDUFA7 (CG3621)	(Murari et al., 2022)[23]	NA
Rabbit anti-dNDUFA8 (CG3683)	(Murari et al., 2021)[24]	NA
Rabbit anti-dNDUFA9 (CG6020)	(Murari et al., 2022)[23]	NA
Rabbit anti-dNDUFA10 (CG6343)	This study	NA
Rabbit anti-dNDUFA11 (CG9350)	(Murari et al., 2021)[24]	NA
Rabbit anti-dNDUFA12 (CG3214)	(Murari et al., 2020)[25]	NA
Rabbit anti-dNDUFA13 (CG3446)	(Murari et al., 2022)[23]	NA
Rabbit anti-dNDUFAB1 (CG9160)	This study	NA
Rabbit anti-dNDUFB1 (CG18624)	(Murari et al., 2022)[23]	NA
Rabbit anti-dNDUFB2 (CG40472)	(Hossain et al., 2022)[22]	NA
Rabbit anti-dNDUFB3 (CG10320)	(Hossain et al., 2022)[22]	NA
Rabbit anti-dNDUFB4 (CG12859)	(Hossain et al., 2022)[22]	NA
Rabbit anti-dNDUFB5 (CG9762)	(Murari et al., 2020)[25]	NA
Rabbit anti-dNDUFB6 (CG13240)	(Murari et al., 2020)[25]	NA
Rabbit anti-dNDUFB7 (CG5548)	(Hossain et al., 2022)[22]	NA
Rabbit anti-dNDUFB8 (CG3192)	(Murari et al., 2020)[25]	NA
Rabbit anti-dNDUFB9 (CG9306)	(Hossain et al., 2022)[22]	NA
Rabbit anti-dNDUFB10 (CG8844)	(Hossain et al., 2022)[22]	NA
Rabbit anti-dNDUFB11 (CG6008)	(Hossain et al., 2022)[22]	NA
Rabbit anti-dNDUFC2 (CG12400)	(Hossain et al., 2022)[22]	NA
Rabbit anti-dNDUFS4 (CG12203)	(Murari et al., 2022)[23]	NA
Rabbit anti-dNDUFS5 (CG11455)	(Murari et al., 2020)[25]	NA
Rabbit anti-dNDUFS7 (CG9172)	(Murari et al., 2021)[24]	NA
Rabbit anti-dNDUFS8 (CG3944)	(Murari et al., 2021)[24]	NA
Rabbit anti-dNDUFV1 (CG9140)	(Murari et al., 2020)[25]	NA
Rabbit anti-dNDUFV2 (CG5703)	(Murari et al., 2022)[23]	NA
Rabbit anti-dNDUFV3 (CG11752)	(Murari et al., 2021)[24]	NA
Rabbit anti-dND1 (CG34092)	(Murari et al., 2020)[25]	NA

REAGENT or RESOURCE	SOURCE	IDENTIFIER
Rabbit anti-dND2 (CG34063)	(Murari et al., 2020)[25]	NA
Rabbit anti-dND3 (CG34076)	(Murari et al., 2020)[25]	NA
Rabbit anti-dND4L (CG34086)	(Murari et al., 2020)[25]	NA
Rabbit anti-dND5 (CG34083)	(Murari et al., 2020)[25]	NA
Rabbit anti-dND6 (CG34089)	(Murari et al., 2020)[25]	NA
Rabbit anti-dHsc70-5 (CG8542)	(Murari et al., 2022)[23]	NA
Rabbit anti-dHsp22 (CG4460)	(Murari et al., 2022)[23]	NA
Rabbit anti-dHsp10A (CG11267)	(Murari et al., 2022)[23]	NA
Rabbit anti-dLonP1 (CG8798)	(Murari et al., 2022)[23]	NA
Rabbit anti-dSTARD7 (CG6565)	This study	NA
Rabbit anti-dTAZ (CG8766)	This study	NA
Chemicals, peptides, and recombinant proteins		
Sucrose	Fisher Scientific	Cat #: S5-500
Magnesium Chloride	Fisher Scientific	Cat #: M33-500
Tris Base	Fisher Scientific	Cat #: BP152-1
Bis-Tris	Fisher Scientific	Cat #: BP301-100
Tricine	Fisher Scientific	Cat #: BP315-100
Sodium Phosphate Monobasic	Fisher Scientific	Cat #: S397-500
Sodium Phosphate Dibasic	Fisher Scientific	Cat #: S375-500
Sodium Chloride	Fisher Scientific	Cat #: S271-1
Hydrochloric Acid	Fisher Scientific	Cat #: SA55-100
Methanol	Fisher Scientific	Cat #: A412-1
Methanol (for lipidomics experiments)	MilliporeSigma	Cat #: 439193
Chloroform	MilliporeSigma	Cat #: 650498
Acetonitrile	MilliporeSigma	Cat #: 34851
Formic Acid	MilliporeSigma	Cat #: 5.33002
Ammonium Formate	MilliporeSigma	Cat #: 70221
2-Propanol	MilliporeSigma	Cat #: 34863
Glutaraldehyde	MilliporeSigma	Cat #: G5882
Osmium Tetroxide	MilliporeSigma	Cat #: 75632
Cacodylic Acid	MilliporeSigma	Cat #: 20835
Acetone	MilliporeSigma	Cat #: 270725
Lead (II) Citrate Tribasic Trihydrate	MilliporeSigma	Cat #: 15326
Paraformaldehyde	Electron Microscopy Sciences	Cat #: 19202
Uranyl Acetate	Electron Microscopy Sciences	Cat #: 22400
EMbed 812 Resin	Electron Microscopy Sciences	Cat #: 14120
Glacial Acetic Acid	Fisher Scientific	Cat #: A38SI-212
Digitonin	MilliporeSigma	Cat #: D141
G-250 Blue Dye	Invitrogen	Cat #: BN2004
NativePAGE Sample Buffer	Invitrogen	Cat #: BN2003
NativePAGE Cathode Buffer Additive (20X)	Invitrogen	Cat #: BN2002

REAGENT or RESOURCE	SOURCE	IDENTIFIER
DNase I	Invitrogen	Cat #: 18-068-015
Bradford 1X Dye Reagent	Bio-Rad	Cat #: 5000205
Halt Protease Inhibitor Cocktail	Thermo Scientific	Cat #: 78430
BSA	Fisher Scientific	Cat #: BP9703-100
Nitrotetrazolium Blue Chloride	MilliporeSigma	Cat #: N6876
Nicotinamide Adenine Dinucleotide Hydrate	MilliporeSigma	Cat #: N7004
Adenosine Triphosphate	Acros Organics	Cat #: 102800100
Sodium Succinate	MilliporeSigma	Cat #: W327700
Phenazine Methosulfate	MilliporeSigma	Cat #: P9625
3,3′-Diaminobenzidine Tetrahydrochloride Hydrate	MilliporeSigma	Cat #: D5637
Cytochrome C	MilliporeSigma	Cat #: C2506
Glycine	Fisher Scientific	Cat #: G46-500
Magnesium Sulfate	Fisher Scientific	Cat #: M65-500
Lead Nitrate	MilliporeSigma	Cat #: 228621
Cardiolipin Mix I	Avanti Polar Lipids	Cat #: LM6003
Mouse SPLASH LIPIDOMIX mass spec standard	Avanti Polar Lipids	Cat #: 330710X
Critical commercial assays		
Novex Colloidal Blue Staining Kit	Invitrogen	Cat #: LC6025
SilverXpress Silver Staining Kit	Invitrogen	Cat #: LC6100
iScript cDNA Synthesis Kit	Bio-Rad	Cat #: 1708891
Amplex Red Hydrogen Peroxide/Peroxidase Assay Kit	Invitrogen	Cat #: A22188
Phosphatidylcholine Assay Kit	MilliporeSigma	Cat #: MAK049
SuperSignal West Pico PLUS Chemiluminescent Kit	Thermo Scientific	Cat #: PI34577
Deposited data		
Raw lipidomics data	This paper	Deposition number: MassIVE MSV000092254
Experimental models: Organisms/strains		
D. melanogaster strain expressing GAL4 in muscles under control of the *mef2* promoter – yw^{1118}; Dmef2-GAL4	(Ranganayakulu et al., 1996)[30]	Dmef2-Gal4
D. melanogaster strain expressing GAL4 in muscles under control of the *mhc* promoter – w*; P{w [+mC]=Mhc-RFP.F3-580}2, P{w [+mC]=Mhc-GAL4.F3-580}2/SM6b	Bloomington Drosophila Stock Center	BDSC 38464; Flybase: FBst0038464
D. melanogaster strain expressing GAL80 under the control of the alphaTub84B promoter – w [*]; P{w{+mC]=tubPGAL80[ts]}10; TM2/TM6, Tb[1]	Bloomington Drosophila Stock Center	BDSC 7108; Flybase: FBst0007108
D. melanogaster strain expressing a transgenic RNAi construct to dSTARD7 (CG6565) – 6565R-1 (RNAi-1)	National Institute of Genetics, Japan	NIG 6565R-1; Flybase: NA
D. melanogaster strain expressing a transgenic RNAi construct to dSTARD7 – w^{1118}; P{GD11963}v39006/TM3 (RNAi-2)	Vienna Drosophila Resource Center	VDRC v39006; Flybase: FBst0462796
D. melanogaster strain expressing a transgenic RNAi construct to dTAZ (CG8766) – y^1 v^1; P {TRiP.JF01564}attP2 (RNAi-1)	Bloomington Drosophila Stock Center	BDSC 31099; Flybase: FBst0031099

REAGENT or RESOURCE	SOURCE	IDENTIFIER
D. melanogaster strain expressing a transgenic RNAi construct to dTAZ – y^1 v^1; P {TRiP.HMC03231}attP2 (RNAi-2)	Bloomington Drosophila Stock Center	BDSC 51484; Flybase: FBst0051484
D. melanogaster strain used as a wild-type control – w^{1118}	Bloomington Drosophila Stock Center	BDSC 3605; Flybase: FBst0003605
Oligonucleotides		
Primers for qPCR, see Table S2	This paper	NA
Software and algorithms		
GraphPad Prism 9	GraphPad	RRID: SCR_002798
LipidSearch 5.0	Thermo Fisher Scientific	RRID: SCR_023716
Other		
Light Contrast Microscope	Olympus	Cat #: SZ61
Forceps	Fine Science Tools	Cat #: 11251-10
Power Supply	Fisher Scientific	Cat #: FB300Q
Bullet Blender	Next Advance	Cat #: BBX24B
Zirconium Oxide Beads	Next Advance	Cat #: ZROB05
NativePAGE 3-12%, Bis-Tris Gel	Invitrogen	Cat #: BN1003BOX
Restek Ultra C18 Reversed Phase HPLC Column, 3 μm	Fisher Scientific	Cat #: 06-739-228
Forma Environmental Chamber	Thermo Fisher Scientific	Cat #: 13-067-066
Mini Gel Tank	Invitrogen	Cat #: A25977
ChemiDoc Gel Imaging System	Bio-Rad	RRID: SCR_019684
Drosophila Activity Monitor	TriKinetics	RRID: SCR_021798
CM12 Transmission Electron Microscope	Philips	RRID: SCR_020411
CFX96 Real-Time PCR Detection System	Bio-Rad	RRID: SCR_018064
Q Exactive HF-X Hybrid Quadrupole-Orbitrap MS System	Thermo Fisher Scientific	RRID: SCR_020558